

Quinones for Aqueous Organic Redox Flow Battery: A Prospective on Redox Potential, Solubility, and Stability

Fuead Hasan,* Vivekananda Mahanta, and Ahmed Adel Abdelazeez

In recent years, there has been considerable interest in the potential of quinones as a promising category of electroactive species for use in aqueous organic redox flow batteries. These materials offer tunable properties and the ability to function as both positive and negative electrolytes, making them highly versatile and suitable for a range of applications. Ongoing research has focused on improving the stability, solubility, and performance of quinones, with a particular emphasis on the creation of stable negolytes. The pairing of these advancements with alternate chemistries has created new prospects for commercial applications. However, challenges persist regarding the stability of quinones in high-potential electrolytes and the limited number of viable quinones available. Despite these obstacles, significant strides have been made, and the potential for quinones to revolutionize energy storage technology is vast. This review article provides a comprehensive overview of recent progress in this area, with a specific focus on redox potential, solubility, and stability, and offers valuable insights into the future of quinone-based aqueous organic redox flow batteries.

address the challenge of balancing the fluctuating supply and demand of energy, there is a growing demand for grid-scale energy storage systems.^[10–13] One promising solution is redox flow batteries (RFBs), which can store electrochemical energy and serve as a bridge between energy generation and consumption.^[14–16] However, conventional RFBs use inorganic materials and corrosive electrolytes, making them less than ideal for widespread adoption.^[17–19] Herein, the high efficiency, cost-effectiveness, and scalability of aqueous organic redox flow batteries (AORFBs) have positioned them as a promising technology for large-scale energy storage.^[20,21] Unlike traditional inorganic-based RFBs, AORFBs utilize organic molecules as the active species, which are earth-abundant and can be easily tailored during synthesis.^[22]

First, organic molecules have a wider range of oxidation states, resulting in higher redox potentials and energy densities.^[23] In addition, organic molecules can be designed and synthesized to have specific properties such as high potential, solubility, and high stability, tailored organic molecules enabling further optimization of the battery's performance.^[24,25] Moreover, aqueous electrolytes used in AORFBs are nonflammable, nontoxic, further enhancing their safety and making them suitable for use in large-scale energy storage applications and less corrosive than traditional inorganic-based RFBs, which allows environmental benefits and cost-effectiveness of the batteries. In recent years, significant progress has been made in the development of AORFBs. Several research groups have demonstrated high energy dense efficient and stable performance of AORFBs in laboratory-scale devices.^[26,27] Further research is ongoing to optimize the design and performance of AORFBs, with the aim of commercializing them for use in large-scale energy storage applications. Although energy density does not matter much in case of flow batteries as they are preferentially being used for stationary applications. However, higher energy density provides additional advantage for batteries. The theoretical energy density can be calculated from the following equation:^[28] Energy density (Wh L⁻¹) = $nCFV/v$ where n is the number of electrons involved in the redox process, C is the concentration of the redox-active species (mol L⁻¹), F is the Faraday constant, V is the cell voltage, and v is the volume electrolyte. This statement does not consider in case of different volumes of catholyte and anolyte. From the above equation, it is evident that the energy density of the flow battery depends on cell

1. Introduction

The growing demand for renewable energy has made it imperative to have efficient grid-scale energy storage systems in place.^[1–4] World's population and economy continue to grow, so too does our reliance on fossil fuels, which has led to environmental damage and climate change. Although renewable energy sources such as solar and wind power have become more affordable in recent years, their intermittent nature presents challenges when it comes to meeting energy demands.^[5–9] To

F. Hasan, A. A. Abdelazeez
 Nanoscale Science
 Department of Chemistry
 The University of North Carolina at Charlotte
 Charlotte, NC 28223, USA
 E-mail: fhasan1@unc.edu

V. Mahanta
 Department of Chemistry
 Indian Institute of Technology Madras
 Chennai 600036, India

 The ORCID identification number(s) for the author(s) of this article can be found under <https://doi.org/10.1002/admi.202300268>

© 2023 The Authors. Advanced Materials Interfaces published by Wiley-VCH GmbH. This is an open access article under the terms of the Creative Commons Attribution License, which permits use, distribution and reproduction in any medium, provided the original work is properly cited.

DOI: 10.1002/admi.202300268

voltage, the solubility of the electroactive species, and the number of electron transfer involves during the redox reaction. The voltage of a cell can be addressed as the modulus of difference in redox potentials of the posolyte and the negolyte. To increase the cell voltage, it is pivotal that the redox potential of the posolyte to have a higher positive value (regardless of whether it is positive or negative), while the redox potential of the negolyte should have a lower negative value (regardless of whether it is positive or negative).^[29,30] The cell voltage can be increased by choosing appropriate redox couples with proper functionalization. The solubility of a substance is regulated by the chemical and physical properties of both solute and solvent. The change in entropy during solvation can give an indication of the solubility. Organic molecules can be tailored to change their properties, so the solubility of redox-active organic molecules with a suitable redox potential is hot area of ongoing research. Various classes of organic molecules have been explored to develop an efficient and stable AQRBFs.^[31] Carbonyls and aza-aromatics are among the classes that have been extensively researched due to their aromatic π systems, which offer higher stability and electrochemical reversibility by allowing delocalization of radical ionic states during redox reactions.^[32] Quinones belong to a class of metal-free organic compounds known for their remarkable electrochemical reversibility, high reaction rates, and strong redox activity. These compounds share a common feature of a six-membered ring system with carbonyl groups, positioned either in *para* or *ortho* configuration, depending on the carbon atom location on the ring.^[33] The potential chemical space for quinones is enormous, presenting a promising opportunity for discovering and designing high-performance AQRFB electrolyte candidates, which can advance the commercialization of advanced redox flow batteries.^[34] Those compounds are earth-abundant, making them attractive for the preparation of potentially cost effective RFBs that can be synthetically tuned. However, the use of quinones can be limited due to stability issues, low solubility, and low operating voltages, which can restrict their widespread application.^[35,36] The solubility of these compounds is frequently contingent upon the pH level, and their solubility can be restricted at a neutral pH. Attempting to increase their solubility by introducing acid or base may lead to a considerable decrease in stability, as they can undergo several chemical reactions, such as Michael addition, epoxidation, nucleophilic attack, dimerization, and tautomerization.^[37]

Research on quinones for AQRFBs has focused on overcoming these limitations and developing an all-organic aqueous redox system.^[38,39] This has involved molecular engineering and the use of electrolyte additives to enhance solubility and stability. Over the past five years, numerous articles have been published on quinone based aqueous flow batteries. This review article delves into the fascinating world of quinone-based redox flow battery design and discovery. By analyzing existing experimental, molecular, and electrochemical analysis methods, this article explores how the core quinone motif has been studied and the techniques used to estimate performance descriptors and understand structure–property relationships. While significant progress has been made in this field, the article also highlights gaps in knowledge and methodology within traditional approaches, and offers suggestions for improvement. Overall, this article provides valuable insights into the cutting-edge world of quinone-based redox flow battery design and discovery, and offers

exciting possibilities for the future of energy storage technology (Scheme 1).

2. Key Parameters to be Considered for Designing Organic Molecules

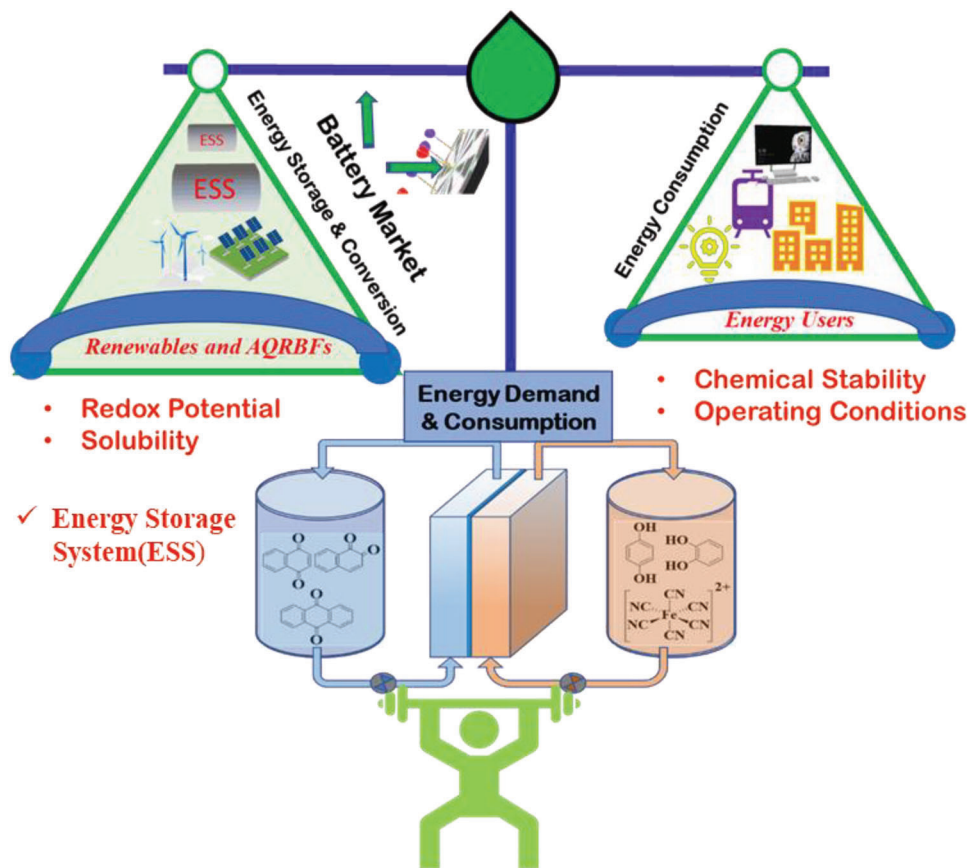
2.1. Redox Potential

The Nernst equation is a useful tool for determining the redox potential of a substance, which indicates its propensity to undergo oxidation or reduction reactions. Redox-active electrolytes can be classified into two groups based on the polarity of their redox potential values: anolytes or negolytes, which can have negative or positive redox potentials, and catholytes or posolytes, which can also have either negative or positive redox potentials. The strength of the redox potential corresponds to the material's capacity to either accept or release electrons. Since the redox potential is a critical property of redox-active materials that affects the battery's open-circuit voltage, there has been significant research ongoing.^[40] If protons or hydroxyl ions are absorbed or released during the redox reaction, the potential is pH-dependent. The redox potential of the species is significantly influenced by the substituents on its parent structure.^[41]

Thus, redox-active species containing EWG possess a higher redox potential than those containing EDG groups.^[42] Therefore, the redox potential can be manipulated using proper substitution. Computational study (density functional theory [DFT], machine learning [ML], etc.) can be used to predetermine effect of substituents on the redox potentials. For instance, Suleyman Er et al. reported an extensive DFT study on different types of quinones benzoquinones (BQ), anthraquinones (AQ), naphthoquinones (NQ), anthraquinone-2,6-disulfonate (AQDS), 4,5-dihydroxybenzene-1,3-disulfonic acid (BQDS) and their derivatives and predicted their redox potentials.^[43] Based on the redox potential, the 9,10-AQ and their derivatives are suitable for anolyte; on the other hand, 1,2-BQ, 1,4-BQ, 2,3-NQ, 2,3-AQ and their derivatives are appropriate for catholyte, which has been well-proved by experimental reports. Leung et al. suggested that LUMO level [calculated using the B3LYP hybrid functional, 6-31+G(d, p) basis set] and redox potentials are linearly related as shown in **Figure 1**, regardless of molecular group.

2.2. Solubility

Assessing the solubility of organic redox-active molecules is challenging as they are often organic salts that dissolve after ion solvation and ionic bond breakage, making their solutions unique from other dissolved species.^[44,45] To prevent clogging of the felt electrodes and ensure maximum utilization of the electrolyte, it is crucial to avoid the precipitation of organic redox-active molecules during battery charging.^[46] Various methods have been developed to address this issue, including the proper selection of the counterion, functionalizing the redox moiety with solubilizing groups, and so on.^[47] The solubility of redox-active molecules can also be determined through computational calculations before synthesis-experimental computations support the



Scheme 1. Schematic diagram summarizing the quinone-based electrolyte chemistries for RFBs discussed in this review.

experimental analysis while also reducing the amount of time required for progress. For example, Leung et al. calculated the ΔG_{sol} values [calculated using the B3LYP hybrid functional, 6-31+G(d, p) basis set and polarizable continuum model] of different organic molecules and tried to relate with the experimental solubility in deionized water. Although it showed a weak corre-

lation with all types of organic molecules, it seems to be linearly fit with the similar types of molecules (BQ, AQ, NQ and their derivatives) (Figure 2). Irregular relations between different types of organic molecules could be due to inability to consider certain solute–solvent interaction such as hydrogen bonding, solvent reorganizations, and so on, by the model.

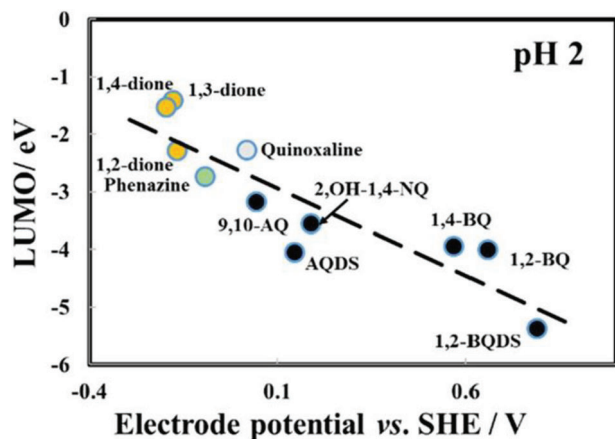


Figure 1. LUMO energies versus experimental redox potentials. Reproduced with permission.^[27] Copyright 2020, Elsevier.

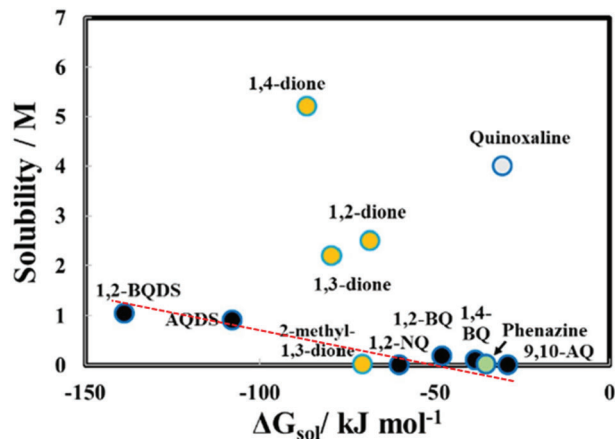


Figure 2. Solubilities versus ΔG_{sol} for different organic molecules. Reproduced with permission.^[27] Copyright 2020, Elsevier.

2.3. Stability

The stability of redox-active species in AQRFBs is crucial for their performance and longevity. Unstable species can deteriorate over time, leading to decreased battery efficiency and shorter lifespan. This stability is also important for the commercial success of AQRFBs, as it affects their ability to compete with other energy storage technologies in terms of cost and performance.^[48,49] The stability of the species is crucial for ensuring that AORFBs can meet the requirements of real-world applications, as unstable species may hinder their viability and cost-effectiveness as energy storage solutions. One of the commonly used methods to evaluate stability is through testing the redox-active material in a symmetric cell, which minimizes the impact of crossover and allows for capacity loss to be attributed solely to precipitation or material decomposition. However, charged species tend to be less stable due to their higher reactivity. To ensure the stability of the electrolyte, it should be tested over time in a flow cell during battery cycling. In situ and in operando analysis are the most effective ways to study and monitor electrolyte degradation, although these techniques are complex and not widely available in all laboratories.^[50–52]

3. Exploring the Relationship between Quinone Structures (BQ, NQ, AQ) and Their Properties for Aqueous Redox Flow Battery Applications

The redox properties of quinone compounds are closely linked to their chemical structure, and these properties can be modified by incorporating specific functional groups.^[53] An electron-withdrawing group (EWG) is a substituent that has a higher electronegativity than the atoms it is attached to. Examples of common EWGs include nitro ($-\text{NO}_2$), cyano ($-\text{CN}$), carbonyl ($-\text{C}=\text{O}$), and halogens ($-\text{F}$, $-\text{Cl}$, $-\text{Br}$, $-\text{I}$). These groups tend to withdraw electron density from the rest of the molecule, including the redox site.^[54,55] This withdrawal of electron density can enhance the positive charge or reduce the negative charge on the redox site, making it more electron-deficient. As a result, the

redox potential of the molecule may shift to a higher value, making it more favorable for electron acceptance (reduction) or less favorable for electron donation (oxidation). On the other hand, an electron-donating group (EDG) is a substituent that donates electron density to the rest of the molecule, including the redox site. Examples of common EDGs include amino ($-\text{NH}_2$), hydroxyl ($-\text{OH}$), alkyl groups ($-\text{R}$), and methoxy ($-\text{OCH}_3$).^[56,57] These groups can increase the electron density on the redox site, making it more electron-rich. Consequently, the redox potential of the molecule may shift to a lower value, making it more favorable for electron donation (oxidation) or less favorable for electron acceptance (reduction) (Figure 3).

It is important to note that these effects are general trends, and the actual influence of EWGs or EDGs on the redox properties of a molecule can depend on the specific molecular structure, solvent environment, and other factors.

The energy level of the lowest unoccupied molecular orbital (LUMO), which ultimately determines the reduction potential. Quinones can exist in different oxidation states, affecting their color, reactivity, and stability.^[58] Solubility is influenced by substituents, with hydrophilic groups improving solubility in polar solvents. Stability is essential for long-term RFB performance, and investigations focus on identifying quinone structures that resist degradation and retain their redox properties.^[59] Overall, understanding the structure–property relationships of quinones facilitates the design of tailored molecules for optimized performance in redox flow batteries.

4. Benzoquinones

4.1. Redox Potentials

Catechol (1,2-dihydroxybenzene) and its derivatives are known for their electrochemical reversibility to a certain degree, with relatively high electrode potentials in aqueous solutions, mostly in acidic conditions.^[61] One example of a redox-active compound with a high standard reduction potential is 1,2-benzoquinone-3,5-disulfonic acid (BQDS), which has two electron-withdrawing

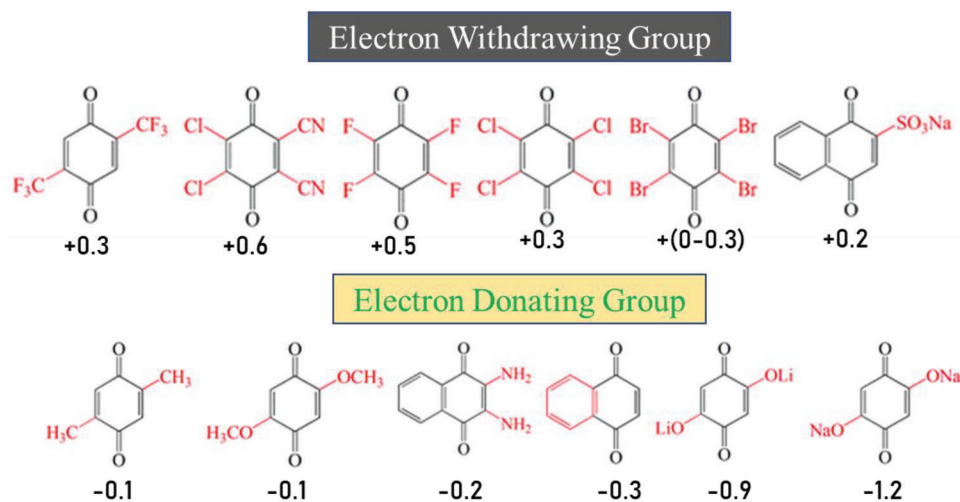


Figure 3. Examples of the working voltage change (ΔE) after introduction of the representative electron-withdrawing and electron-donating groups. Reproduced with permission^[60] Copyright 2018, Elsevier.

groups ($-\text{SO}_3\text{H}$) that contribute to its high potential experimentally (+1.1 V) vs normal hydrogen electrode (NHE) with compare to +0.67 V of hydroquinone. Murali et al. investigated the potential of 3,6-dihydroxy-2,4-dimethylbenzenesulfonic acid (DHDMBS) as a redox-active compound for use in aqueous organic RFBs. DHDMBS was found to have a standard reduction potential of +0.85 V versus NHE, making it a promising candidate for use in RFBs.^[62] In acidic conditions, the morpholinomethylene group gets protonated and behaves as EWG instead of EDG, resulting in higher redox potential of morpholinomethylene substituted hydroquinones.^[52,63]

4.2. Solubility

The solubility of hydroquinone, hydroquinone sulfonic acid, and BQDS are 0.53, 0.8, and 1 M, respectively. Two sulfonic groups on the benzene ring improve the solubility of BQDS.^[64] Functional groups like $-\text{OH}$, $-\text{NH}_2$, $-\text{COOH}$, $-\text{SO}_3\text{H}$, and $-\text{PO}_3\text{H}_2$ are useful in increasing the water solubility. However, as $-\text{OH}$ and $-\text{NH}_2$ are electron-donating groups, these decrease the redox potential of hydroquinone/benzoquinone. It is worth noting that the specific impact of substituent groups on solubility and redox potential can vary depending on the molecular structure, the presence of other functional groups, and the surrounding solvent environment. For example, the incorporation of electron-withdrawing groups $-\text{COOH}$, $-\text{SO}_3\text{H}$, and $-\text{PO}_3\text{H}_2$ can offer advantages in terms of both solubility and redox potential. Therefore, a comprehensive understanding of the molecular design principles and thorough experimentation are necessary to optimize the performance of redox-active molecules for catholyte applications

4.3. Stability

Benzoquinones are susceptible to the Michael addition of nucleophiles at the unsubstituted sites. Addition of any nucleophilic group addition changes the molecule's redox potential. For instance, H_2 -BQDS gets oxidized to its BQDS during the charging process in a flow battery operation, which further goes through a series of Michael addition of water molecules (Figure 4). The introduction of substituted products resulting from the Michael reaction leads to a reduction in the cell voltage of the system. The presence of each electron-donating $-\text{OH}$ group substitution causes a decrease in the molecule's reduction potential by 100 mV per electron-donating group.^[65]

Murali et al. claim that during charge–discharge cycling, the solubilizing group ($-\text{SO}_3\text{H}$) is removed from DHDMBS, resulting in insoluble 2,6-dimethylbenzene-1,4-diol (Figure 5). Surprisingly, although DHDMBS has an unsubstituted site, Michael addition of water was claimed to be absent by the author.

2-Methoxy-1,4-hydroquinone (MHQ) produced from vanillin (4-hydroxy-3-methoxybenzaldehyde) was used in acidic AQRFB by Schlemmer et al.^[66] MHQ is highly unstable in acidic and alkaline environments and is also UV-sensitive. In solution, it easily dimerizes to produce insoluble byproducts. Quinoid radical production during operation leads to degradation. However, they were able to achieve rather good performance with a capacity retention of around 87% after 250 cycles by utilizing 0.5 M H_3PO_4

as the supporting electrolyte, which is known to be a stabilizing agent for a range of organic compounds and radical scavengers.

Several researches have demonstrated the rapid polymerization of dopamine in alkaline environments. Furthermore, in 0.5 M H_2SO_4 , dopamine exhibits a reversible redox peak at $\approx +0.77$ V versus standard hydrogen electrode (SHE).^[67] Hence, Liu et al. examined dopamine feasibility as catholyte in AQRFBs, which upon cycling the capacity was degraded 50% within 100 galvanostatic charge–discharge.^[67] Although the capacity decay was mitigated to some extent ($\approx 82\%$ after 200 GCD cycling) using saturated NH_4Cl in the catholyte, the mechanism of mitigating capacity decay is unknown. Schindler et al. and Mahanta et al. proposed that dopamine undergo electrochemical polymerization through radical formation at the unsubstituted sites of dopamine in acidic medium (Figure 6).^[68,69] It was believed based on the studies mentioned above that fully protected hydroquinone with four bulky substituents would be stable for RFB with a lengthy cycle life. Hence, Mahanta et al. reported a fully substituted dopamine by three $-\text{Br}$ group and tested in a flow battery. The rate of capacity degradation was found to be only $\approx 0.028\%$ cycle⁻¹ for 2500 galvanostatic charge–discharge cycles.^[70] This was capacity fade triggered due to crossover induced precipitation of redox active species and hydrogen evolution.^[71,65]

Dražević et al. report underscores the significance of protonation in modulating the electrochemical properties of the fully substituted hydroquinone molecule. The ability to control the protonation degree opens avenues for fine-tuning the molecule's redox potential and optimizing its suitability for specific applications in various electrochemical systems. This group proposed tetramorpholinomethylene substituted hydroquinone to demonstrate this hypothesis. However, capacity retention of the symmetric cell was realized to be only 33% after 100 GCD cycles. The cross-over of the active species, electrolyte imbalance, and chemical instability of the species could be the possible reason for the capacity loss.^[72] Yang et al. studied four morpholinomethylene and/or methyl group substituted hydroquinones (HQ6–HQ9) Figure 7 as catholyte in the acidic medium in a symmetric flow battery to better understand the impact of substituents on the stability of such hydroquinones. The hydroquinone molecule with two bulky morpholinomethylene groups (HQ6) and two unprotected *ortho* positions exhibited a significant capacity loss, amounting to 71% within a mere two-day period. On average, this corresponds to a capacity decay rate of 0.235% cycle⁻¹ over the course of 300 cycles. The observed capacity loss indicates that the morpholinomethylene groups, although possessing a significant steric hindrance due to their bulkiness, were insufficient in completely protecting the hydroquinone molecules from undesired reactions. HQ7 still showed capacity reduction of 7.3% d⁻¹ ($= 0.190\%$ cycle⁻¹ for 263 cycles in the symmetrical cell) despite being entirely substituted. HQ8 and HQ9 showed capacity deterioration of 0.87% d⁻¹ ($\approx 0.099\%$ cycle⁻¹) and 0.45% d⁻¹ ($\approx 0.058\%$ cycle⁻¹ for 223 cycles), respectively. Both of these reports^[62] concluded that the morpholino group decomposes to produce an insoluble precipitate based on the post cycle study. The latter report did not analyze the Michael addition of H_2O in HQ6 or the reduced capacity that may have resulted from a smaller degree of morpholino-group breakdown in HQ7–HQ9. Park et al. proposed a high voltage acid-based RFB with a four (dimethylamino)methyl group substituted 1,4-hydroquinone (HQ10) as

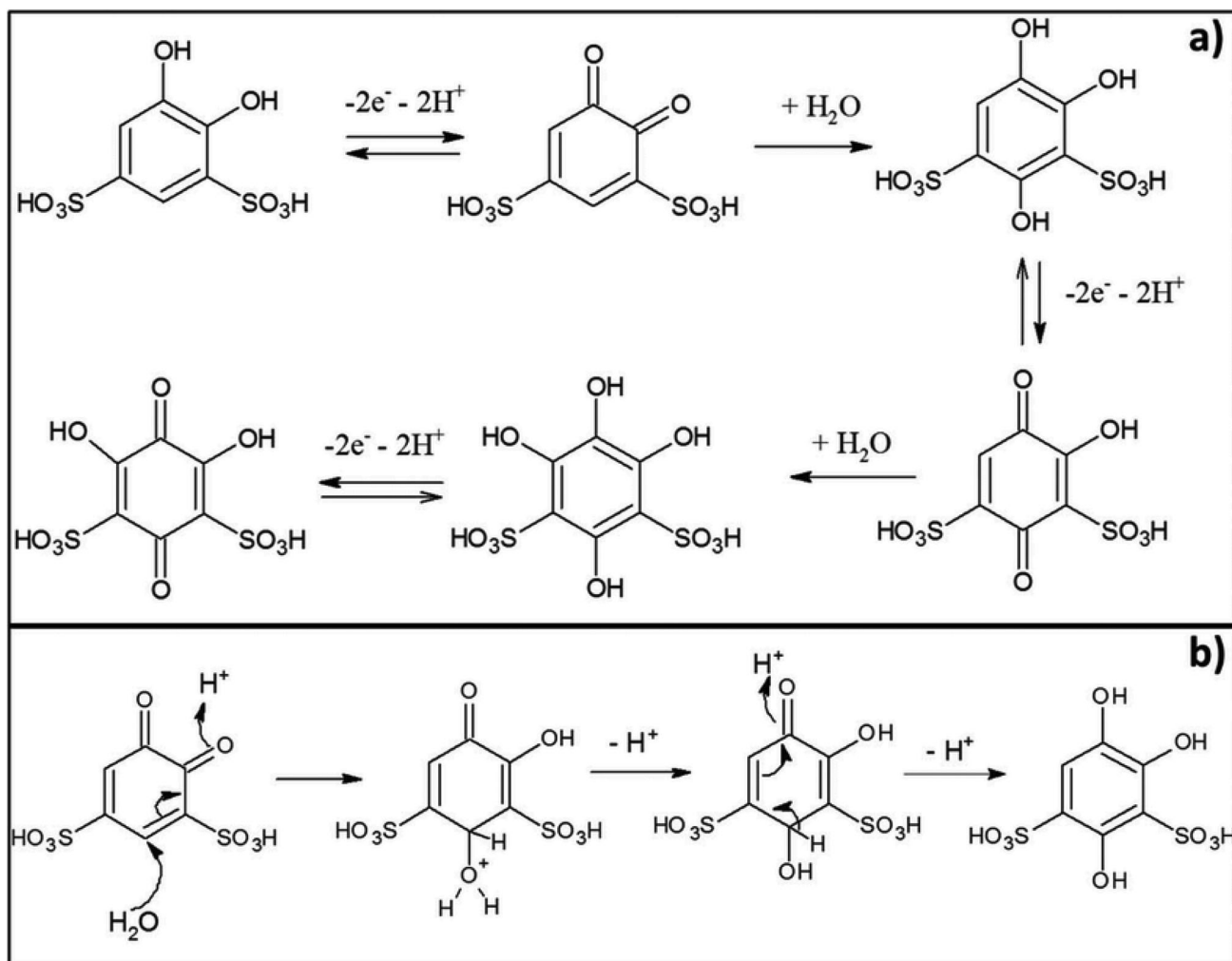


Figure 4. a) Reaction steps in the transformation of BQDS during charging; b) reaction scheme for the Michael reaction showing the nucleophilic addition of water followed by rearomatization and proton exchange.^[65]

catholyte and $Zn/[Zn(OH)_4]^{[73-75]}$ as anolyte material.^[76] Even though the RFBs cycling demonstrated a capacity retention rate of 99.93% cycle⁻¹ for 50 cycles, which implies chemical stability needs to be investigated after a higher number of cycles. On the otherhand using 2,5-bis((dimethylamino)methyl)benzene-

1,4-diol (HQ11) in 3 M H_2SO_4 as catholyte was proposed by Sivanadanam et al.^[77] The capacity degradation of the RFB was observed to be exceptionally high, resulting in a limited lifespan of only 15 cycles before significant performance deterioration occurred. After subjecting the catholyte to a galvanostatic charge–discharge (GCD) process, it was stored for a duration of 10 d. Subsequently, a cyclic voltammetry (CV) study was conducted, revealing the emergence of two additional peaks situated below the redox potential of the primary redox peak. These additional peaks signify the occurrence of a chemical conversion process wherein the parent electroactive species transformed into electron-rich electroactive species. According to the report, the observed degradation could potentially be attributed to the formation of gem-diol compounds and the Michael addition of water. To prevent such decomposition, the researchers have proposed two fully substituted hydroquinone derivatives. The first derivative, named HQ12, features two methyl groups positioned in a *para* configuration to each other, along with two (dimethylamino)methyl groups also in a *para* configuration. The second derivative, HQ13, includes four (4-methylpiperazin-1-yl) methyl groups.

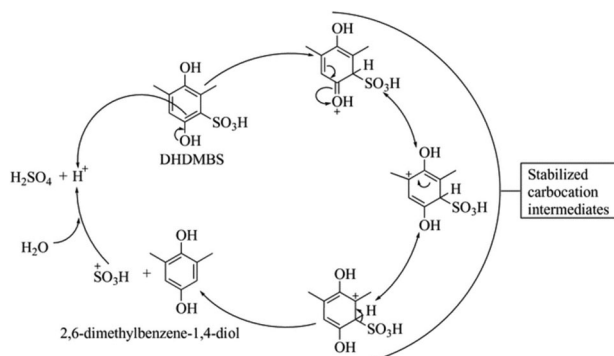


Figure 5. Decomposition of DHDMBS via proto-desulfonation.^[62]

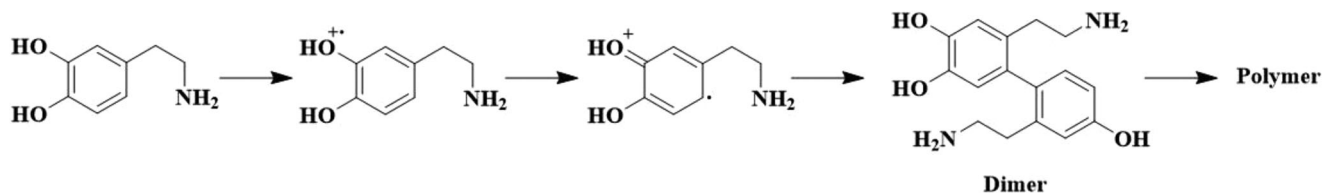


Figure 6. Electrochemical-induced degradation mechanism of dopamine in acidic medium.^[66]

These proposed derivatives, **HQ12** and **HQ13**, Figure 7 aim to enhance the stability of the hydroquinone molecule by strategically substituting it with specific groups. **HQ12** structural arrangement of methyl and (dimethylamino)methyl groups, both in a *para* configuration, is designed to mitigate degradation pathways. Similarly, **HQ13** incorporates four (4-methylpiperazin-1-yl) methyl groups, which are expected to contribute to the stability and protection of the hydroquinone core. Employing these fully substituted hydroquinone derivatives, the researchers seek to overcome the challenges associated with degradation, ensuring the sustained integrity and longevity of the electrochemical system. Further exploration and characterization of **HQ12** and **HQ13** will shed light on their potential as promising alternatives in achieving enhanced stability and performance in redox-active systems. However, their stability in flow cell needs to be studied further.^[78,79]

5. Naphthoquinones

5.1. Redox Potential

The redox potential of bislawsone in 1 M KOH is -0.551 V versus SHE. The reduction potential of bislawsone is 50 mV more negative to lawsone monomer with overlapping peaks for the two

subunits, which states that bislawsone is more suitable as anolyte in RFB.^[80]

5.2. Solubility

The solubility of lawsone is 0.48 M (0.96 M electrons), whereas it is 0.56 M (2.24 M electrons) in pH 14 solution. The nonplanar structure of the dimer along the 3,3'-single bond disrupt crystal packing and hence solubility higher than the monomer (lawsone).^[80] The increased solubility of the dimer is in contrast with the usually decreased solubility of many extended polymers compared to their parent monomers.^[81]

5.3. Stability

Wedge et al. reported that, similar to benzoquinones, naphthoquinones are also vulnerable to Michael addition reaction. As KOH solution is used as electrolyte medium, the nucleophile (OH^-) is even stronger than the H_2O in acidic/neutral medium. According to the report, the capacity of the lawsone-based RFBs declines rapidly (Figure 6a). In RFB configurations, there is a possibility of contamination by trace amounts of oxygen, which can lead to the generation of highly reactive superoxide species and

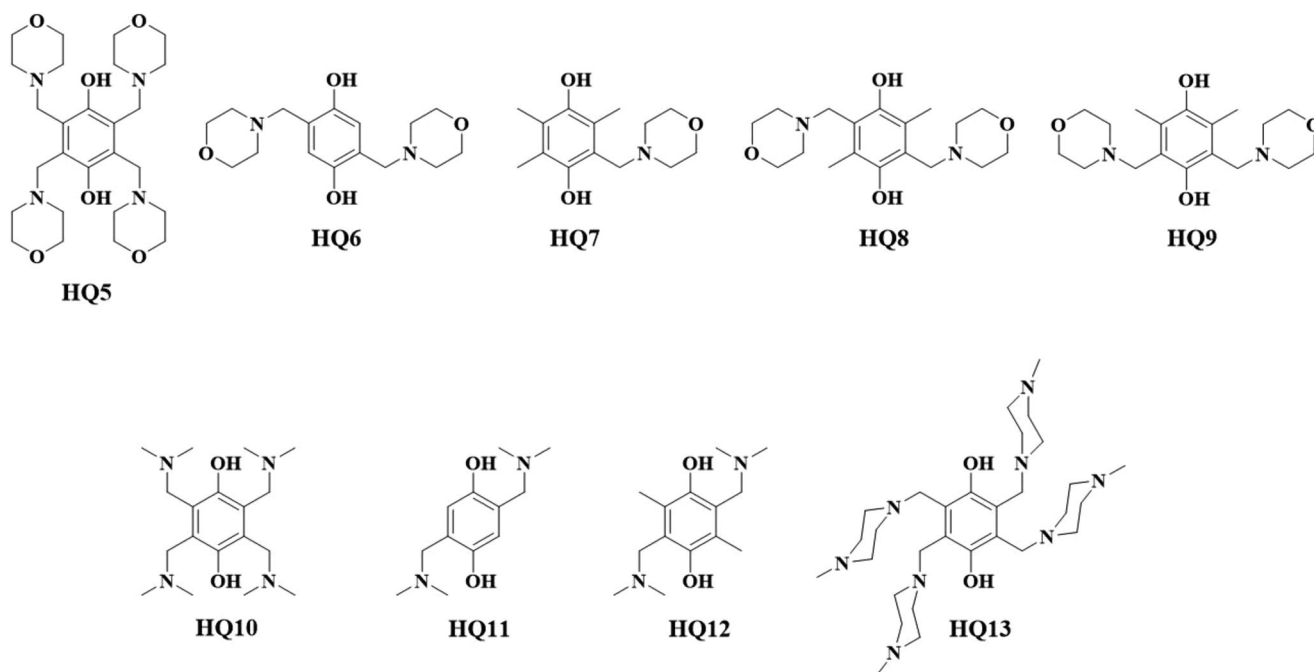


Figure 7. Hydroquinone with nitrogen-based functional group.

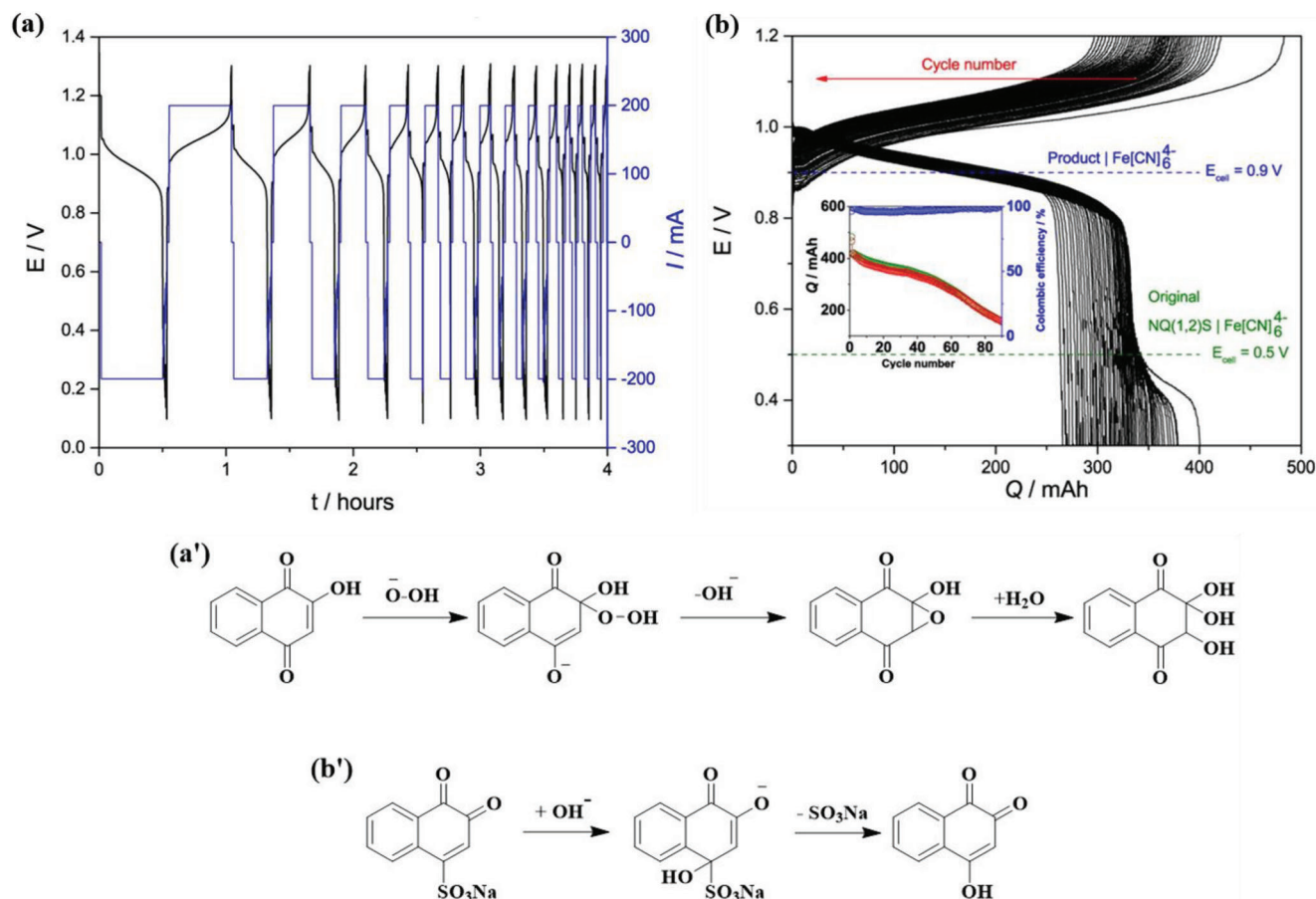


Figure 8. Charge–discharge profile of the RFB with a) 0.2 m lawsone, b) 0.2 m Folin's reagent solutions in 1 m KOH. The inset of (b) shows the capacity (green for charging and red for discharging) and coulombic efficiency (blue). Degradation pathway of a') lawsone and b') Folin's reagent.^[42]

hydrogen peroxide upon interaction with hydroquinone compounds. In alkaline solutions, the formation of hydrogen peroxide and its corresponding anion further amplifies their nucleophilic properties, surpassing even the reactivity of the hydroxide ion. The presence of superoxide and hydrogen peroxide species resulting from oxygen contamination in RFBs presents a significant challenge that must be carefully addressed during system design and operation. Consequently, it was hypothesized that the hydroquinone molecule undergoes epoxidation through interaction with the hydroperoxide anion, followed by subsequent nucleophilic attack. This chemical transformation gives rise to the formation of non-aromatic and electrochemically irreversible hydroxylated species (Figure 8a'). In general, the presence of multiple hydroxyl groups in quinone compounds often leads to electrochemical irreversibility and/or insolubility, resulting in capacity degradation. However, in a different naphthoquinone-based RFB system, which utilized Folin's reagent (sodium 1,2-naphthoquinone-4-sulfonate), the observed capacity fade was significant but comparatively less than that of lawsone (as shown in Figure 6b). In this particular case, Folin's reagent undergoes desulfonation upon interaction with hydroxide ions, giving rise to the formation of a new redox-active species (Figure 8b').

Hu et al. reported a highly stable lawsone||4-hydroxy-TEMPO RFB system, demonstrating exceptional capacity retention of 99.992% cycle⁻¹ (as shown in Figure 9). In a separate study by

Tong et al., a naphthoquinone dimer called bislawsone was investigated, wherein the sites susceptible to Michael addition were effectively blocked. Despite these modifications, the RFB exhibited a capacity fade rate of 0.74% d⁻¹ when operated at 100 mA cm⁻² for 12.8 d, and 0.78% d⁻¹ when operated at 300 mA cm⁻² for an additional 6.8 d after 1.2 d of rest. The observed capacity fade in the RFB system was attributed to an irreversible keto-enol tautomerism process that occurs during battery operation. This transformation leads to the formation of an insoluble, redox-inactive material. The accumulation of this material over time contributes to the gradual decrease in capacity (Figure 10).

6. Anthraquinones

6.1. Redox Potential

In a study conducted by Jing et al., the influence of substituents' chains and ionic end groups on the redox potentials of AQs was investigated. The study revealed that the redox potentials of AQs possessing two unsaturated hydrocarbon chains are affected by the presence of electron-withdrawing end groups, which exhibit an influence through π -conjugation. Moreover, in the case of chains consisting of two (un)saturated straight hydrocarbons, the order of water solubilizing groups in terms of increasing the redox potentials of AQs was found to be: PO₃²⁻ < CO₂⁻ < SO₃⁻.

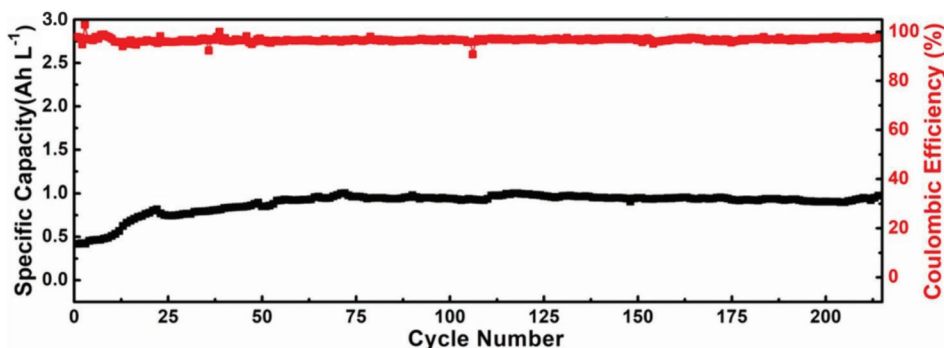


Figure 9. Long cycle performance of RFB with 0.1 M lawsone with 15 mA cm^{-2} current density. Reproduced with permission.^[82] Copyright 2017, American Chemical Society.

From **Figure 11**, it is clear that COOH group with saturated-branched hydrocarbons shows the lowest redox potential and hence suitable for anolyte purpose.^[83,84] Most of the reported AQs are reversible in alkaline medium. However, some of the quinizarin and alizarin are reversible in acidic medium (0.1 M HClO_4). Quinizarin and alizarin are notable examples of bifunctional analytes due to their characteristic of exhibiting two distinct redox signatures that are separated by $\approx 1 \text{ V}$ vs NHE. This unique feature makes them suitable candidates for utilization as both catholyte and anolyte materials in RFBs.^[85] By leveraging their dual redox behavior, these compounds offer the flexibility to operate in different electrochemical states, enabling efficient energy storage and conversion within the RFB system. The ability to function as both catholyte and anolyte expands the versatility and applicability of quinizarin and alizarin in the field of energy storage and offers potential advantages in designing and optimizing RFB configurations.^[86,87]

6.2. Solubility

Mao et al. studied the effect of position of substituents and counter cation on the solubility of anthraquinone sulfonate salts (2,7-AQDS²⁻, AQS⁻, 1,5-AQDS²⁻) in water.^[88] It was found that

the solubility of a salt apparently depends on the following a trend of $\text{Mg}^{2+} > \text{Na}^+ > \text{K}^+ > \text{Ca}^{2+} > \text{Ba}^{2+}$, and the quinone anion with a trend of 2,7-AQDS²⁻ \gg 1,5-AQDS²⁻ $>$ AQS⁻ (**Figure 12**), (**Table 1**).

The quinizarin and alizarin are barely soluble in water ($\approx 0.004 \text{ M}$) and in acidic medium. **Figure 13** shows the solubility of different quinizarin and alizarin derivatives. The difference in solubilities in these two could be due to difference in symmetry. The asymmetrical nature of alizarin derivatives contributes to their increased dipole moments, reduced crystalline packing, and consequently, higher solubilities. Notably, alizarin S. red protonated (ASR-H) and its counterpart with cation exchange using tetrahydroxyl-phosphonium (ASR-TKMP) exhibit the highest solubilities, reaching $\approx 1.6 \text{ M}$, when dissolved in a 0.1 M HClO_4 solution (**Figure 14**).

Redox-active species based (**Figure 14**) on AQ, the incorporation of hydrophilic groups at the β -sites (2, 3, 6, 7) is anticipated to enhance water-miscibility to a greater extent compared to the α -sites (1, 4, 5, 8).^[90] However, Xia et al. found an anomalous case where α -substituted AQ 3-((9,10-dioxo-9,10-dihydroanthracen-1-yl)amino)-N,N,N-trimethylpropan-1-aminium chloride (1-DPAQCl) has much higher water-solubility than the β -substituted AQ (2-DPAQCl).^[90] In the case of

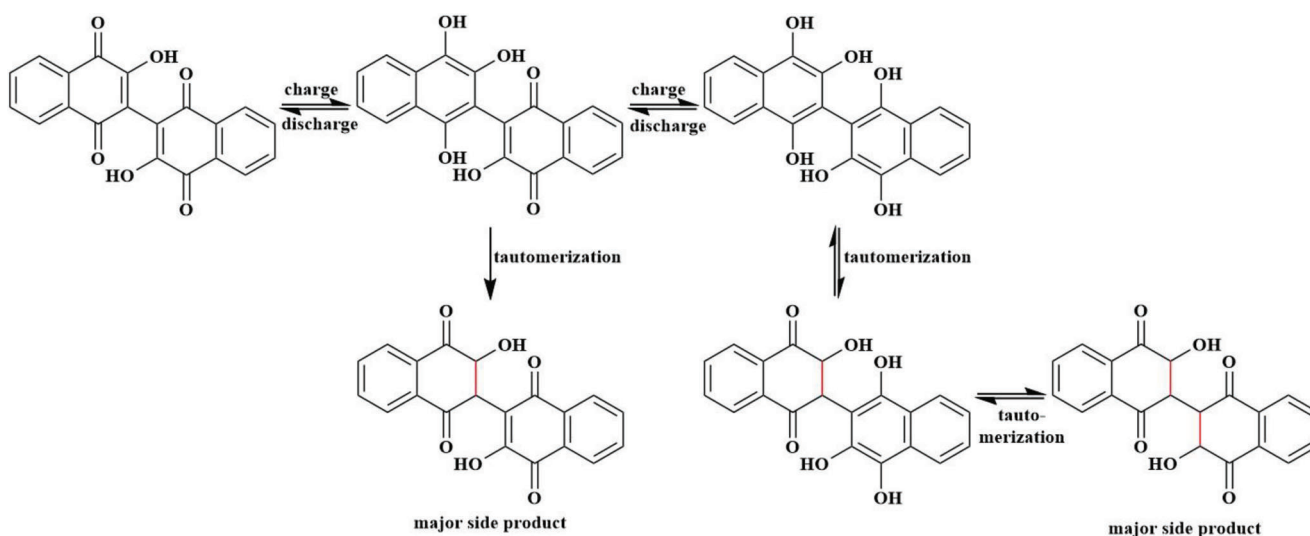


Figure 10. Degradation of bislawsone. Reproduced with permission.^[83] Copyright 2019, American Chemical Society.

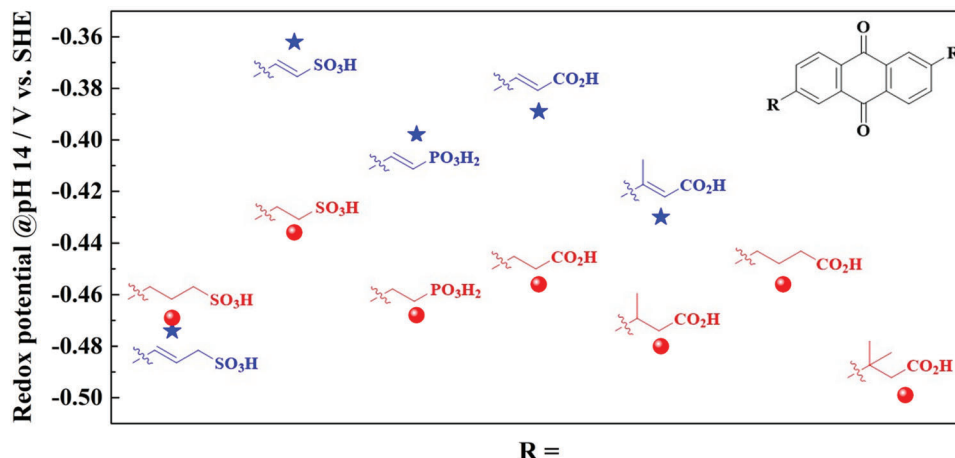


Figure 11. Effect of saturated/unsaturated functional groups on the redox potential of 2,6-anthraquinone.

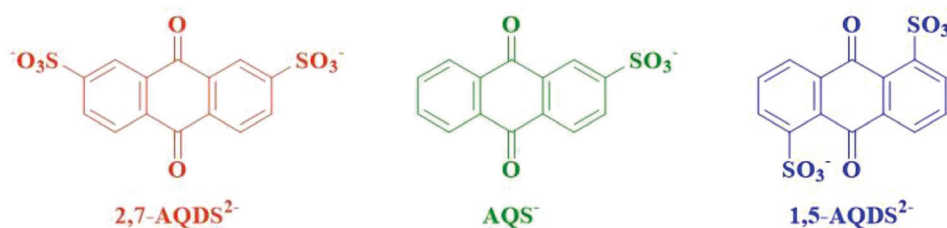


Figure 12. Structure of anthraquinone sulfonate salts (2,7-AQDS²⁻, AQS⁻, 1,5-AQDS²⁻).^[88]

2-DPAQCl, intermolecular hydrogen bonding occurs between the NH donor of the substituent, as depicted in the figure above. Conversely, in 1-DPAQCl, an intramolecular hydrogen bond forms between the NH donor of the α -substituent and the O=C acceptor. Due to the presence of intramolecular hydrogen bonds, the interaction between solute molecules in 1-DPAQCl is more susceptible to disruption by water compared to that in 2-DPAQCl. As a result, 1-DPAQCl exhibits enhanced water solubility. The presence of intermolecular hydrogen bonds can hinder water solvation by requiring more energy to disrupt the bonds and surround the free Cl⁻ with water molecules. This effect is more pronounced at higher concentrations. On the other hand, the N-H group of 1-DPAQCl is immobilized by its neighboring C=O acceptor, allowing water molecules to more easily disrupt the attraction between the ions in a manner similar to that of NaCl. Consequently, the solubility of 1-DPAQCl significantly increases to 1.44 M. In general, functional groups such as -SO³⁻, -CO²⁻, and PO³²⁻ are effective solubilizing groups for anthraquinones. However, it should be noted that these groups are electron-withdrawing in nature,

which can raise the redox potential of AQ. This increase in redox potential is not desirable for an anolyte application in a redox flow battery. Therefore, direct attachment of these functional groups to AQ is not recommended in order to maintain the desired redox potential suitable for anolyte utilization. Wang et al. reported N,N'-(9,10-anthraquinone-2,6-diyl)-di- β -alanine (DAEAQ) where the substituent is attached to AQ through electron-donating amine. The solubility of DAEAQ was measured to be 0.99 M in 1 M KOH, where -COOH act as the solubilizing group.^[91] Guiheneuf et al. introduced a novel compound called 2,3-dihydroxylated anthraquinone (2,3-DHAQ) with a notable solubility of 0.7 M in KOH at pH levels above 13.5.^[92] Another study conducted by Jing et al., the influence of functional groups with saturated/unsaturated bonds on the solubility of 2,6-anthraquinone (2,6-AQ) was investigated. The study revealed that under pH 12 conditions, functional groups such as -CO₂H and -PO₃H₂ are fully deprotonated, resulting in high solubilities of the corresponding compounds (Figure 15). Interestingly, the unsaturated versions of AQ demonstrated lower solubilities compared to their saturated counterparts, as

Table 1. Solubilities measured via UV-vis spectroscopy (error \approx 4.7%).

AQ derivatives	Na ⁺	K ⁺	Mg ²⁺	Ca ²⁺	Ba ²⁺
2,7-AQDS ²⁻	0.740 M	0.380 M	1.26 M	0.0201 M	0.0018 M
AQS ⁻	0.0197 M	0.0193 M	0.0644 M	0.0025 M	0.000945 M
1,5-AQDS ²⁻	0.0720 M	0.010 M	0.0838 M	0.00149 M	0.000311 M

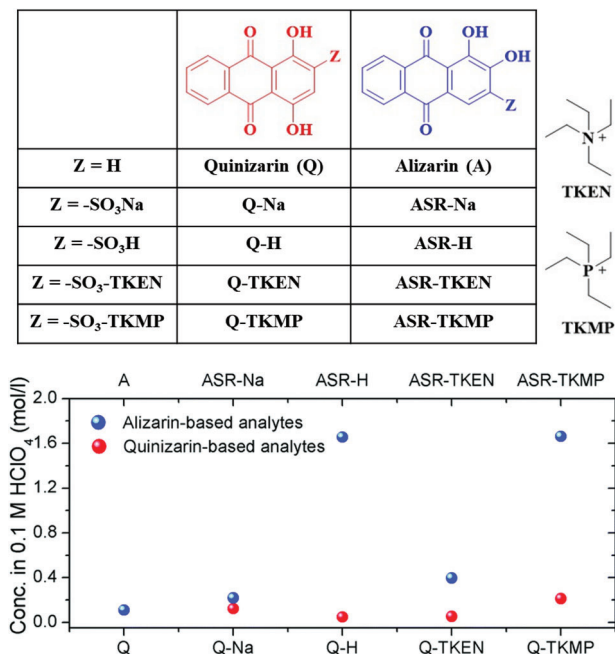


Figure 13. Solubilities of different quinizarin and alizarin derivatives. Reproduced with permission.^[85] Copyright 2016 The Royal Society of Chemistry.

depicted in Figure 11. This finding highlights the significance of functional groups and their saturation state in governing the solubility properties of 2,6-anthraquinone derivatives. This is attributed to the extended conjugation in unsaturated AQs, which enhances the intermolecular π - π interactions, thereby reducing their solubility in water.^[93] Wu et al. reported that the solubility of 1,8-dihydroxy-2,7-dicarboxymethyl-9,10-anthraquinone (DCDHAQ) is 1.3 M, which is much higher than its precursor 1,8-DHAQ (<0.02 M).^[94] The solubility of 3,3'-(9,10-anthraquinone-diyl)bis(3-methylbutanoic acid) (DPivOHAQ) and 4,4'-(9,10-anthraquinone-diyl)dibutanoic acid (DBAQ) at pH 12 are 0.74 and 1.0 M, respectively.^[95] According to the findings of Lee et al., the addition of ethylene glycol as an additive was found to enhance the solubility of 2,7-anthraquinone disulfonic acid (2,7-AQDS) in a KCl solution. Specifically, the solubility increased from 0.3 to 0.8 M. Importantly, this increase in solubility did not negatively impact the electrochemical performance of the system.^[96]

6.3. Stability

The compound 2,6-dihydroxyanthraquinone (2,6-DHAQ) demonstrates a notable drawback of high capacity fade due to the formation of an electrochemically inactive anthrone dimer. This undesirable reaction significantly reduces the capacity and performance of the system over time.^[97] However, a method to regenerate 2,6-DHAQ electrochemically was employed. This involved performing an additional discharge step down to a voltage of -0.1 V at regular intervals, typically every 50 cycles. This regeneration process helped mitigate the capacity fade issue and allowed for the sustained electrochemical activity of 2,6-DHAQ

in the system (Figure 16). Guiheneuf et al. have recently introduced 2,3-dihydroxylated anthraquinone (2,3-DHAQ) as a novel compound for RFB applications. In their study, they subjected 2,3-DHAQ to an extensive cycling regime, performing up to 3000 charge-discharge cycles. This investigation aimed to assess the electrochemical stability and long-term performance of 2,3-DHAQ as a redox-active material in RFBs (Figure 17). Despite a capacity fade rate of $\approx 0.019\%$ cycle⁻¹, the study revealed that by employing deep discharging (i.e., decreasing the discharge cut-off voltage), it was possible to fully recover the initial capacity. The authors of the study put forward a hypothesis that the capacity degradation observed in 2,3-DHAQ is associated with the formation of anthrone species during cycling. Furthermore, they proposed that oxidation reactions occurring during deep discharge cycles enable the restoration of the initial 2,3-DHAQ structure and consequently the initial capacity (Figure 18).

The direct attachment of solubilizing groups to the aryl rings of redox-active molecules can have a significant impact on their reduction potential (Figure 18), this approach often comes at the expense of molecule lifetime, leading to degradation or instability. On the other hand, when short alkyl linkages are used to separate the solubilizing groups from the aryl rings, the lifetime of the molecule is prolonged. However, this modification tends to limit the shift in reduction potential, ultimately affecting the overall open-circuit voltage (OCV) of the full-cell system. This trade-off between reduction potential and molecule lifetime highlights the challenges faced in designing redox-active molecules with both enhanced solubility and long-term stability. The compounds 4,4'-((9,10-anthraquinone-2,6-diyl)dioxy)dibutyrate (2,6-DBEAQ) and (((9,10-dioxo-9,10-dihydroanthracene-2,6-diyl)bis(oxy))bis(propane-3,1-diyl))bis(phosphonic acid) (2,6-DPPEAQ) have demonstrated a remarkable combination of high operating life, solubility of 1 M electrons, and an OCV of 1.0 V. Specifically, the capacity fade rate of 2,6-DPPEAQ, as reported by Ji et al., is extremely low at $\approx 0.00036\%$ cycle⁻¹, 0.014% d⁻¹, or 5.0% per year. These results highlight the outstanding long-term stability and desirable electrochemical performance of 2,6-DBEAQ and 2,6-DPPEAQ as redox-active materials in relevant applications.^[98] DPivOHAQ and DBAQ (Figure 19) show capacity decay of 0.014% d⁻¹ and 0.0084% d⁻¹ at pH 12, respectively. Anthrone formed (as degraded product) was recovered by air exposure.

Anthraquinones are widely used as anolyte in combination with ferri/ferrocyanide catholyte. In the study conducted by Kwabi et al., it was observed that a symmetric flow battery operated with 2,6-DBEAQ on both sides exhibited a remarkably low capacity fade rate of less than 0.01% d⁻¹ and less than 0.001% cycle⁻¹. However, when 2,6-DBEAQ was used as an anolyte and ferri/ferrocyanide as a catholyte, the flow battery demonstrated a higher temporal capacity fade rate of 0.04% d⁻¹, which was four times higher than that of the symmetric flow battery. The authors proposed a hypothesis that the additional capacity fade observed in the asymmetric setup could be attributed to the precipitation of 2,6-DBEAQ in the positive electrolyte (posolyte) after crossover.^[98,99] In contrast to the substantial temporal fade rate of 5% d⁻¹ observed in the RFB using 2,6-DBEAQ, 2,6-DHAQ has been found to exhibit higher chemical stability, although the exact reasons for this difference are not fully understood. It has been proposed that the stability of 2,6-DHAQ may be attributed

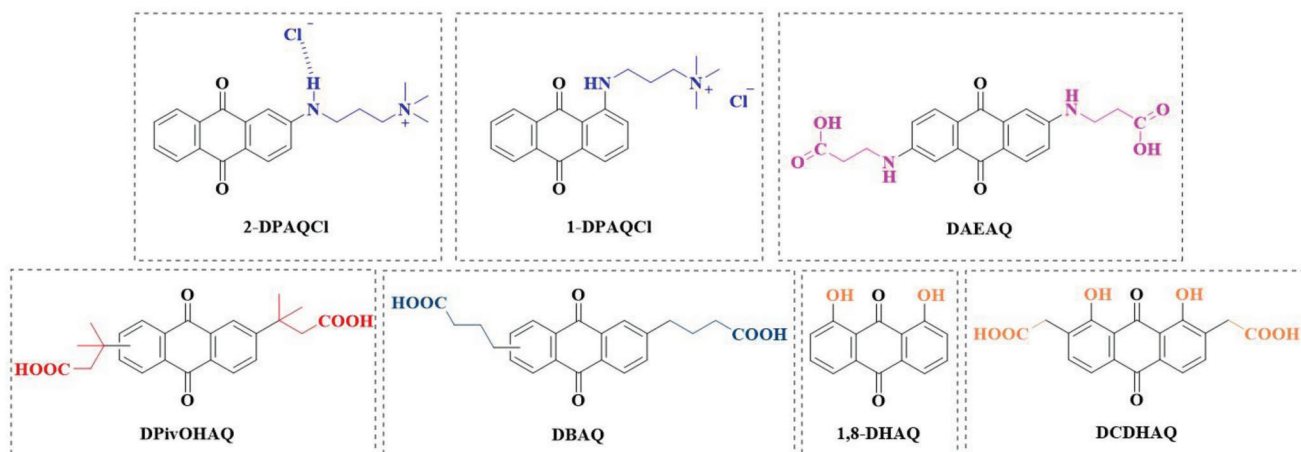


Figure 14. Example of hydrophilic group substituted anthraquinones for aqueous redox flow batteries.

to its reduced forms. While the reduced form of 2,6-DBEAQ is highly unstable even at elevated temperatures, the reduced form of 2,6-DHAQ is relatively stable. Furthermore, the negatively charged deprotonated hydroxyl groups in 2,6-DBEAQ are positioned closer together, leading to increased intramolecular coulombic repulsion forces. This enhanced repulsion may contribute to the instability of the reduced form of the molecule. The observations regarding the stability of 2,6-DHAQ compared to 2,6-DBEAQ highlight the importance of molecular structure and the influence it can have on the chemical stability of redox-active compounds. Furthermore, the susceptibility of 2,6-DBEAQ to the generation of semiquinone radicals, as observed in the CV study, may contribute to its lower stability. While alkyl chain functionalization can extend the lifetime of AQs, it cannot completely prevent decomposition. In the case of 2,6-DHAQ, the scientists discovered that the oxidized form undergoes decomposition through cleavage of the γ -hydroxybutyrate moiety when subjected to elevated temperatures. These findings suggest that the presence of alkyl chains in AQ molecules can enhance their stability to some extent, but under certain conditions, such as in-

creased temperatures, decomposition pathways can still occur. Understanding the decomposition mechanisms and factors influencing the stability of AQ derivatives is crucial for the development of more stable and durable redox-active compounds for flow battery applications. Guiheneuf et al. conducted an extensive study on the degradation of 3,4-dihydroxy-9,10-anthraquinone-2-sulfonic acid sodium salt (ARSNa) during an extended 11-month cycling period. They identified 3-hydroxy-9,10-anthraquinone-2-sulfonic acid (HAQS) as the primary degradation product resulting from a hydrodeoxygenation reaction. This reaction involves the removal of oxygen atoms from the ARSNa molecule, leading to the formation of HAQS. The formation of HAQS as a degradation product suggests that the hydroxy groups in ARSNa undergo chemical transformations during cycling, likely influenced by the reaction conditions and electrolyte environment.^[100,101] The degradation of Alizarin-3-methyliminodiacetic acid (AMA) occurs through the loss of carboxylic groups, resulting in reduced solubility of the active substance and a subsequent decrease in battery capacity.

Chai et al. employed micellization techniques to stabilize anthraquinone compounds in their study on 2,6-poly(ethylene glycol) substituted anthraquinones (PEG n -AQs), where n represents the number of ethylene oxide units in the polymer chain. Their investigation focused on PEG12-AQ, which exhibited an impressive cycle life with an average capacity retention of 99.998% cycle⁻¹ when tested for 3600 charge–discharge cycles over 28 d at a low concentration (0.1 M). At a higher concentration (0.35 M), the battery still demonstrated excellent performance with a capacity retention of 99.98% cycle⁻¹. The outstanding performance of the battery was attributed to the protective effect of the hydrodynamic PEG chains surrounding the AQ framework. These chains acted as a barrier, preventing nuclear attacks from nucleophiles and inhibiting intramolecular dimerization processes that lead to anthrone production. By effectively shielding the AQ molecule, the PEG chains enhanced the stability and prolonged the cycle life of the battery.^[102,103]

The unbalanced state of charge refers to a situation in flow batteries where the charge stored in the catholyte (positive electrolyte) is different from the charge stored in the anolyte (negative electrolyte). This can occur due to various factors such as

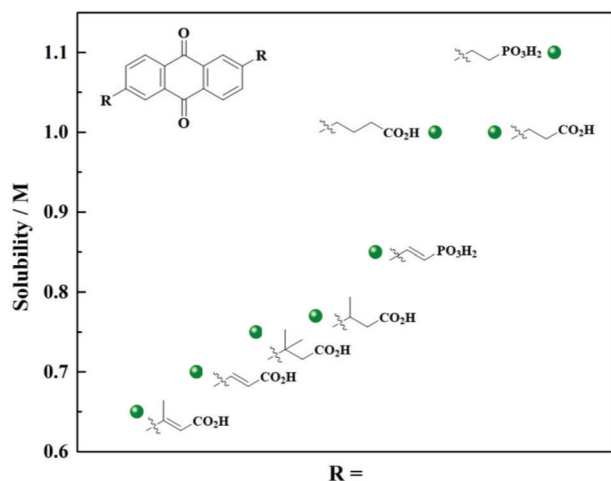


Figure 15. Effect of substituents on solubility of 2,6-AQ.^[89]

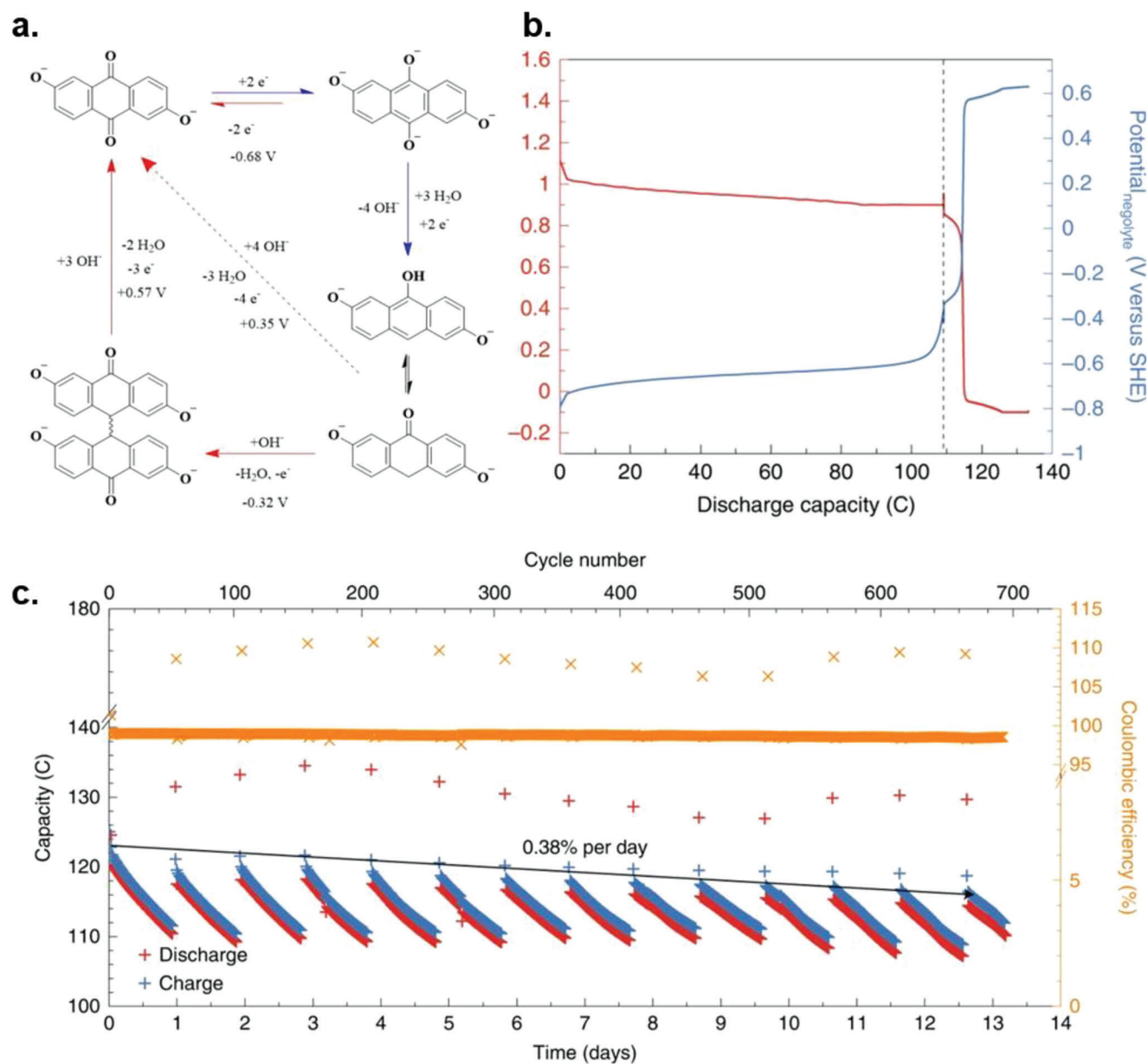


Figure 16. a) Potential-driven DHAQ-related molecular conversions at pH 14, b) electrochemical regeneration step of negolyte, c) repeated application of the electrochemical regeneration step of negolyte in a flow battery (composition: 6.5 mL, 100×10^{-3} M DHAQ²⁻, 1 M KOH in the negolyte, and a mixture of 35 mL, 60×10^{-3} M $K_4[Fe(CN)_6]$ and 30×10^{-3} M $K_3[Fe(CN)_6]$, 1 M KOH in the posolyte). Reproduced with permission. [97] Copyright 2022, Springer Nature.

uneven reactant utilization, electrolyte crossover, or inefficiencies in the charging and discharging processes. Under operational conditions, unintended reactions such as oxygen evolution reaction (OER), hydrogen evolution reaction (HER), and chemical oxidation reactions can irreversibly consume electrons, leading to an unequal state of charge in the catholyte and anolyte of a RFB. This charge imbalance process is illustrated in **Figure 20**, where “A” represents the catholyte and “B” represents the anolyte. The OER occurs at the cathode, where oxygen gas is evolved by consuming electrons from the catholyte. This leads to a decrease in the state of charge in the catholyte. Conversely, the HER takes place at the anode, where hydrogen gas is produced by consum-

ing electrons from the anolyte, resulting in a decrease in the state of charge in the anolyte. In addition, charge imbalance can also occur through chemical oxidation reactions involving reduced species in the negative electrolyte. For example, the presence of oxygen in the solution can chemically oxidize reduced viologen to its oxidized form, consuming electrons and causing a decrease in the state of charge in the negative electrolyte.^[104,105] These charge imbalances can impact the efficiency and performance of the RFB, as they result in a deviation from the desired stoichiometry and can lead to capacity fade and reduced overall energy efficiency. To mitigate these issues, various strategies can be employed, including the use of catalysts to enhance

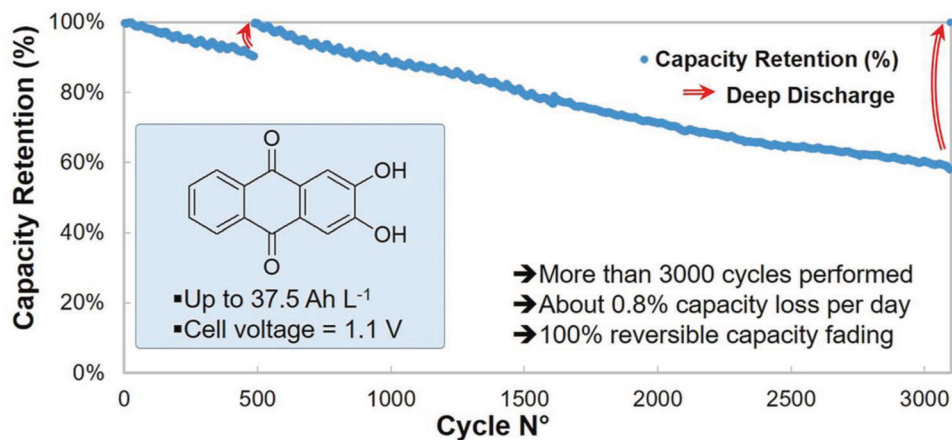


Figure 17. Capacity retention curve demonstrating regeneration of capacity by deep discharge (composition: 40 mL solution of 0.2 M 2,3-DHAQ in 1.8 M KOH as anolyte, and 44 mL solution of 0.5 M potassium ferrocyanide in 0.2 M NaOH as catholyte). Reproduced with permission.^[92] Copyright 2022, Elsevier.

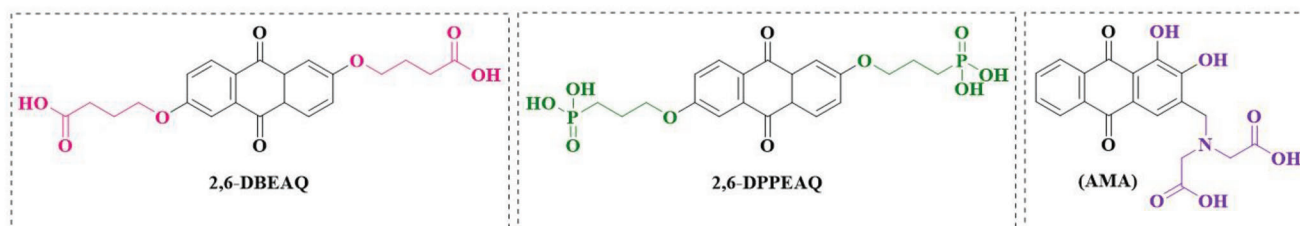


Figure 18. Examples anthraquinones with directly linked solubilizing groups to the aryl rings.

the kinetics of the OER and HER, optimizing electrolyte compositions to minimize chemical oxidation reactions, and implementing proper control algorithms to maintain charge balance between the catholyte and anolyte. The study conducted by Paez et al., an electrochemical balancing process was employed to restore the oxidation states of the two half-cell solutions in a RFB. One of the challenges they addressed was the parasitic oxygen reduction reaction (ORR) at the negative electrode, which caused a severe decline in capacity when the RFB was operated in an open atmosphere. To mitigate this issue, the researchers replaced the oxygen dissolved in the electrolyte with an inert gas such as nitrogen (N₂) or argon (Ar). By doing so, the faradaic imbalance caused by the ORR was reduced. As shown in Figure 21a,b, these were able to restore the capacity by raising the charging cutoff and

deliberately permitting OER.^[106] It should be highlighted that the capacity fading, which is caused by anthrone formation, was still seen in both inert atmosphere and after rebalancing every ten cycles. This approach helped to minimize the unwanted side reactions associated with the presence of oxygen, thus improving the overall performance and capacity retention of the RFB (Table 2).

6.3.1. Electrolytes Requirements

In the operation of RFBs, the electrolyte plays a crucial role as it serves as the medium for electrochemical energy storage and acts as a carrier for the electroactive species.^[107–109] To ensure the efficient performance of RFBs, there are several essential physical

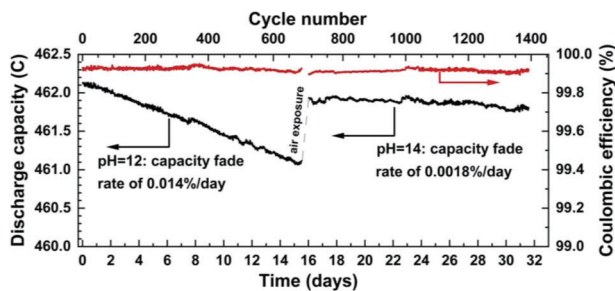


Figure 19. Cycling performance of DPivOHAQ||K₄[Fe(CN)₆] flow battery at pH 12 and 14. Reproduced with permission.^[95] Copyright 2020, Elsevier.

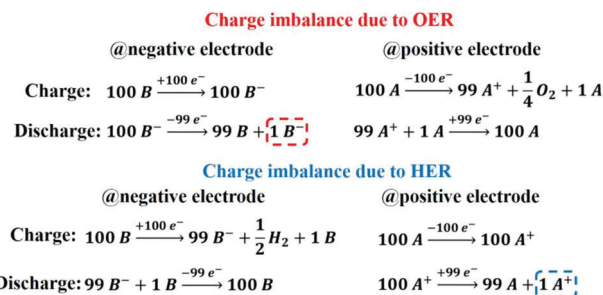


Figure 20. Charge imbalance mechanism in RFBs due to undesirable electrochemical processes.^[102]

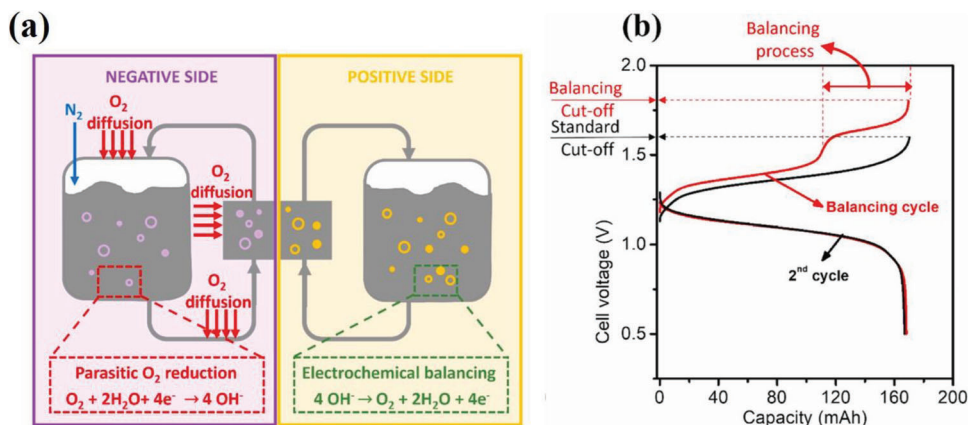


Figure 21. a) Schematic representation of parasitic reaction and electrochemical balancing reaction involved in the DHAQ|| $K_4[Fe(CN)_6]$ RFB, and b) charge–discharge profile showing electrochemical balancing process. Reproduced with permission.^[106] Copyright 2020, Elsevier.

and chemical criteria that the electrolyte needs to meet along with redox potential, solubility, and chemical stability of electroactive quinones.

6.3.2. Wide Electrochemical Potential Window

The energy density of a RFB is influenced by various factors, including the cell potential, which is the potential difference between the standard potentials of the redox couples involved. To achieve a high cell potential, it is desirable to maximize the separation between the redox potentials of the anolyte and catholyte species. However, this separation is constrained by the electrochemical stability range of the solvent. For instance, in the case of water under normal conditions, this gap is limited to 1.23 V, which represents the difference between water oxidation and reduction potentials. Therefore, a larger potential window allows for a wider range of optimization possibilities for new redox species.^[110,111] Recent studies have reported the widening of the electrochemical stability windows of aqueous supporting electrolytes to values greater than 3 V as shown in **Figure 22**.

This has been achieved through the development of “water-in-Li salt” and “water-in-ionic liquid” electrolyte systems.^[108,117] “Water-in-ionic liquid” electrolytes involve the incorporation of

ionic liquids into water to create stable electrolyte solutions with extended electrochemical stability windows.^[118,119] Ionic liquids, which are organic salts with low volatility, can offer higher thermal stability and wider electrochemical stability ranges compared to traditional aqueous electrolytes. When combined with water, these ionic liquids create a hybrid electrolyte system that can tolerate higher voltages without undergoing significant decomposition or side reactions.^[120,121]

6.3.3. Ionic Conductivity

During the charge/discharge process of a RFB, the active species present in the bulk electrolyte need to migrate toward the electrode–electrolyte interface to undergo the redox reactions. Similarly, counter ions must be transported through the membrane to maintain charge balance on both sides of the battery. These processes rely on the efficient mobility of ions, which is facilitated by ionic conductivity. Ionic conductivity refers to the ability of ions to move freely within the electrolyte. It is a crucial property that determines the efficiency of charge transfer and ion transport in RFBs. Higher ionic conductivity allows for faster migration of active species and counter ions, resulting in improved battery performance.^[122,123]

Table 2. Cycle life of some best performing RFBs containing anthraquinone-based anolyte and $K_4[Fe(CN)_6]$ catholyte.

AQ-based anolyte	Operating time/cycle	Cycle fade rate	Ref.
2,6-DHAQ	≈700 cycles (>13 d) with repeated electrochemical regenerative step	0.38% d ⁻¹ with regenerative step	[97]
2,3-DHAQ	3000 cycles with regenerative step: electrochemical – deep discharge	≈0.019% cycle ⁻¹ (≈0.8% d ⁻¹) without regenerative step (deep discharge) and 0% after deep discharge	[92]
2,6-DPPEAQ	480 cycles (12.3 d)	0.00036% cycle ⁻¹ (0.014% d ⁻¹ , 5.0% year ⁻¹)	[92]
DPivOHAQ	15.6 d (690 cycles) at pH 12, and then regeneration by air exposure followed by another 700 cycles at pH 14	0.014% d ⁻¹ at pH 12 and 0.0018% d ⁻¹ at pH 14	[95]
DBAQ	650 cycles (15.5 d) at pH 12	0.0084% d ⁻¹ at pH 12	[95]
2,6-DBEAQ	6 d (≈375 cycles)	0.04% d ⁻¹	[99]
PEG12-AQ	3600 cycles (28.3 d) with 0.1 m and 180 cycles with 0.35 m	0.002% cycle ⁻¹ in case of 0.1 m and 0.02% cycle ⁻¹ in case of 0.35 m	[102]

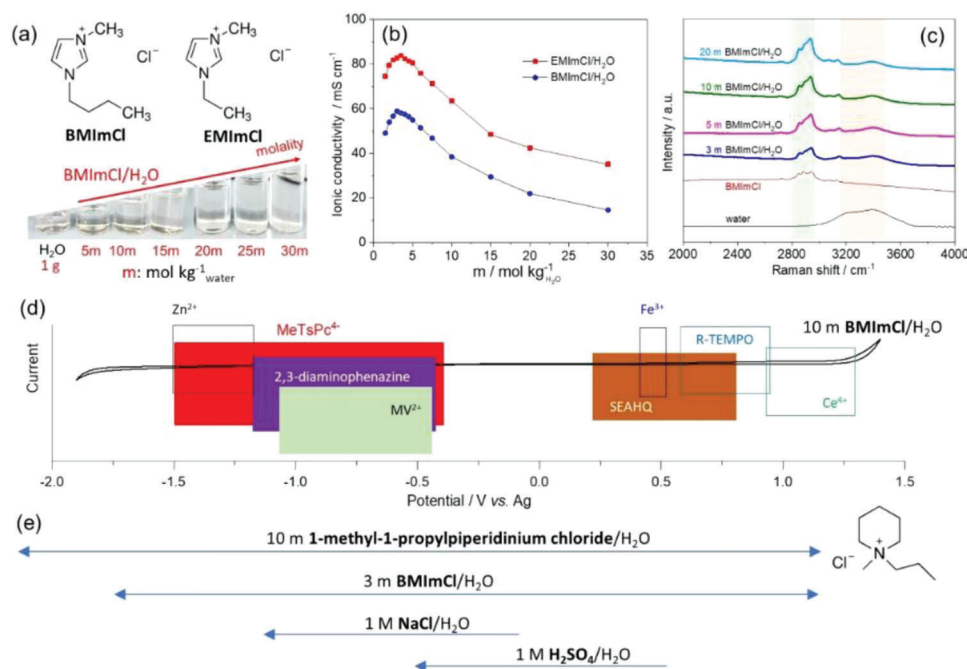


Figure 22. Selected redox couple with “water-in-ionic liquid” electrolytes, a wide electrochemical stability window of ≈ 3 V has been demonstrated. a) Molecular structures of water-miscible ionic liquids BMImCl and EMImCl. b) Graph showing the ionic conductivity of “water-in-ionic liquid” supporting electrolytes. c) Raman spectra of “water-in-BMImCl” electrolytes with different amount of water. d) Electrochemical stability window measured on a glassy carbon electrode for various redox couples (MeTsPc $^{4-}$: transition metal phthalocyanine tetrasulfonic acid anion; MV $^{2+}$: methyl viologen cation; SEAHQ: 2-[(2,5-dihydroxyphenyl) sulfanyl]ethan-1-aminium chloride; R-TEMPO: 4-position substituted TEMPO. e) Comparison of electrochemical stability among aqueous ionic liquids, NaCl, and H $_2$ SO $_4$ electrolytes, emphasizing the onset potentials of the hydrogen evolution reaction (HER). Reproduced with permission.^[114] Copyright 2020, Elsevier. Reproduced with permission.^[115] Elsevier. Reproduced with permission.^[108]

To achieve great mobility and enhance ionic conductivity, various factors come into play. These include the selection of appropriate electrolyte materials, optimization of solvent properties, and the design and characteristics of the membrane (Figure 23). Electrolytes with high ion concentrations and low viscosities promote enhanced ionic conductivity.^[124,125] Solvents with favorable properties such as high dielectric constant and low viscosity can facilitate ion mobility and conductivity. Membranes with high selectivity for ions and low resistance to ion transport are essential for maintaining efficient charge transfer and preventing cross-contamination between the positive and negative electrolyte streams.^[126,127]

By focusing on maximizing ionic conductivity, researchers aim to improve the overall efficiency and performance of redox flow batteries, enabling more effective charge/discharge processes and better utilization of the active species present in the electrolyte.

6.3.4. Viscosity

In RFBs, a continuous flow of electrolyte is used to store energy in external electrolyte reservoirs. The viscosity of the electrolyte plays a significant role in the efficiency of the RFB system. Higher viscosity requires more effort from the pumping system, resulting in reduced energy efficiency and increased pressure drops. Therefore, a low viscosity is desirable to minimize the energy consumption of the device.

Based on the provided graph and data (Figure 24), it can be observed that the viscosity of liquid quinones is influenced by the redox-active electron concentration in various quinone-based electrolytes. The graph compares different liquid quinones, including the naphthoquinone eutectic (NQE) system, benzoquinone eutectic (BQE), and a glycolated naphthoquinone liquid obtained through molecular engineering. The graph highlights the low viscosity of single-component benzoquinones and the BQE mixture in the BQE-Q and BQE-Q/HQ compositions, as indicated in the inset. This suggests that these quinones possess favorable fluidic properties, which can be advantageous for their application in redox flow batteries. Furthermore, the graph also compares the viscosity of liquid quinones with different supporting electrolytes. It includes eutectic quinone mixtures such as NQE-Q: PIL, which represents the oxidized form of NQE mixed with an imidazole-imidazolium TFSl NSPIL, and BQE-Q: AA/W, which indicates a mixture of BQE with acetic acid and water. The comparison also incorporates a molecular engineering approach using a glycolated liquid naphthoquinone with LiTFSI and a solvent-led approach using a vanadium electrolyte V $_2$ (SO $_4$) $_5$.

As the RFB charges and the state of charge (SoC) increases, the composition of the electrolyte changes, which can affect its properties including viscosity.^[128,129] It is crucial to maintain a low viscosity regardless of the level of energy storage to ensure optimal performance throughout the charge/discharge cycles. Viscosity is directly linked to mass transfer processes within the RFB. Geoffroy et al. discovered a relationship between the activation energy of viscous flow and ionic conductivity, with their product

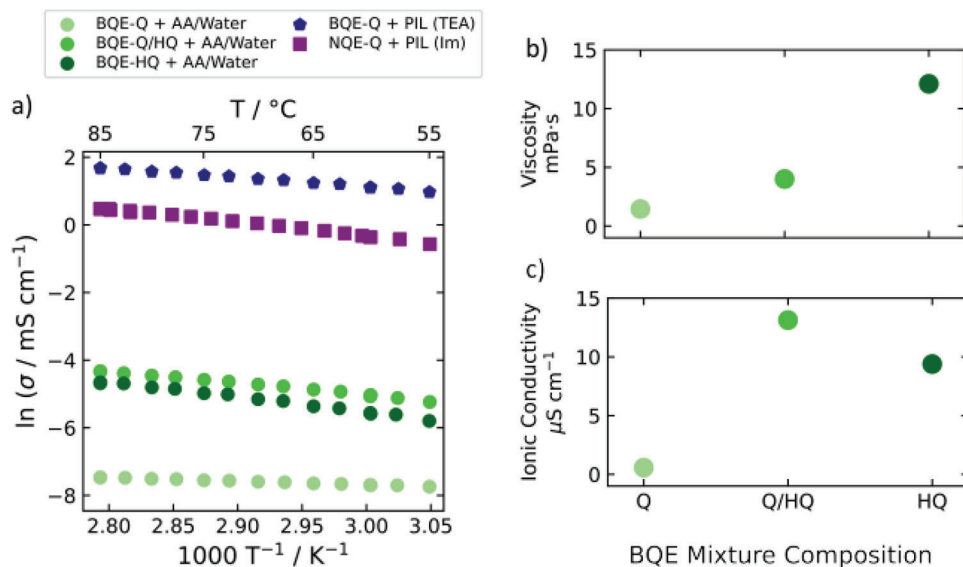


Figure 23. a) The ionic conductivity of eutectic quinone supporting electrolyte mixtures is compared in different compositions. In one study, the ionic conductivity of a benzoquinone eutectic (BQE) system with an acetic acid and water supporting electrolyte (10:5:1 BQE:AA:water) is measured across three states of charge: BQE-Q, BQE-Q/HQ, and BQE-HQ. These represent the quinone form, the 1:1 quinone to hydroquinone form, and the hydroquinone form of the mixture, respectively. It is observed that mixtures with acetic acid supporting electrolyte exhibit lower ionic conductivity compared to those with nonstoichiometric protic ionic liquids (NSPIL) electrolytes. The comparison is made with BQE-Q: protic ionic liquids (PIL) containing triethylamine-triethylammonium (TEA-TFSI) NSPIL supporting electrolyte in a 5:1 BQE:PIL ratio, and NQE-Q: PIL (Im), which consists of imidazole-imidazolium TFSI NSPIL supporting electrolyte in a 5:1 NQE:PIL ratio. b,c) The change in BQE mixture properties with the state of charge is investigated. In the oxidized, quinone-rich composition, the BQE viscosity is minimized, indicating lower resistance to flow (b). On the other hand, the highest ionic conductivity is measured for the 1:1 quinone/hydroquinone mixture, indicating enhanced ion transport within the electrolyte. These measurements were conducted at 85 °C, except for the BQE-Q viscosity, which was measured at 60 °C. Reproduced with permission.^[124] Copyright 2023, American Chemical Society.

remaining constant regardless of temperature. Therefore, an increase in viscosity leads to an immediate decrease in conductivity.

To enhance the efficiency and performance of RFBs, it is essential to minimize viscosity and maintain low viscosity levels throughout the operation. This helps reduce energy consumption, pressure drops, and supports efficient mass transfer, ensuring the smooth functioning of the RFB system.

6.3.5. Supporting Electrolytes

In the context of water as a solvent for RFBs, pure water exhibits low ionic conductivity, resulting in significant ohmic losses during the charge–discharge process. To overcome this limitation, the use of supporting electrolytes becomes necessary.^[130,131] Supporting electrolytes are compounds that can undergo ionization in the solvent, generating both anions and cations. This ionization contributes to improving the overall ionic conductivity of the electrolyte solution. When selecting a supporting electrolyte for water-based RFBs, several requirements need to be considered. One crucial requirement is minimizing the negative impact on the solubility of the active species. It is well-known that the solubility of a solute can be influenced by the presence of other solutes, which can result in excluded volume effects or changes in solution activity.

In the case of water as a solvent, it is important to select supporting electrolytes that have minimal impact on the solubility of the active species. This ensures that the desired redox reactions

can proceed efficiently without compromising the solubility and availability of the active materials. By carefully choosing suitable supporting electrolytes, the ionic conductivity of the water-based electrolyte can be significantly enhanced, leading to improved overall performance and reduced ohmic losses during the charge-discharge process in water-based RFBs.^[22,132,133] In aqueous media, the use of various supporting electrolytes is limited by their solubility characteristics. However, due to the ionic nature of these electrolytes, there is a wide range of possibilities available. This allows for the utilization of cost-effective electrolytes in high concentrations. Examples of such electrolytes include inorganic salts like sodium chloride (NaCl), which has been widely studied in the context of RFBs.^[78,134,135] Strong bases such as potassium hydroxide (KOH)^[136,137] or sodium hydroxide (NaOH)^[138] as well as acids can also be employed.

The miscibility of TFSI-based ionic liquids with liquid quinones has been observed, allowing for enhanced ionic conductivity in the resulting mixture. However, when salts containing the more hydrophilic triflate anion are used, they do not increase the ionic conductivity of the mixture. This lack of conductivity enhancement is hypothesized to be a result of immiscibility between the triflate salts and the liquid quinones. The TFSI anion, when paired with alkali metal salts (Li, Na, and K), has been found to exhibit solubility in the quinone eutectics,^[138,139] specifically benzoquinone and naphthoquinone, which were the focus of our study.^[140,141] This solubility leads to the formation of ionically conductive electrolytes. It is important to note that while these electrolytes are not suitable for proton-based

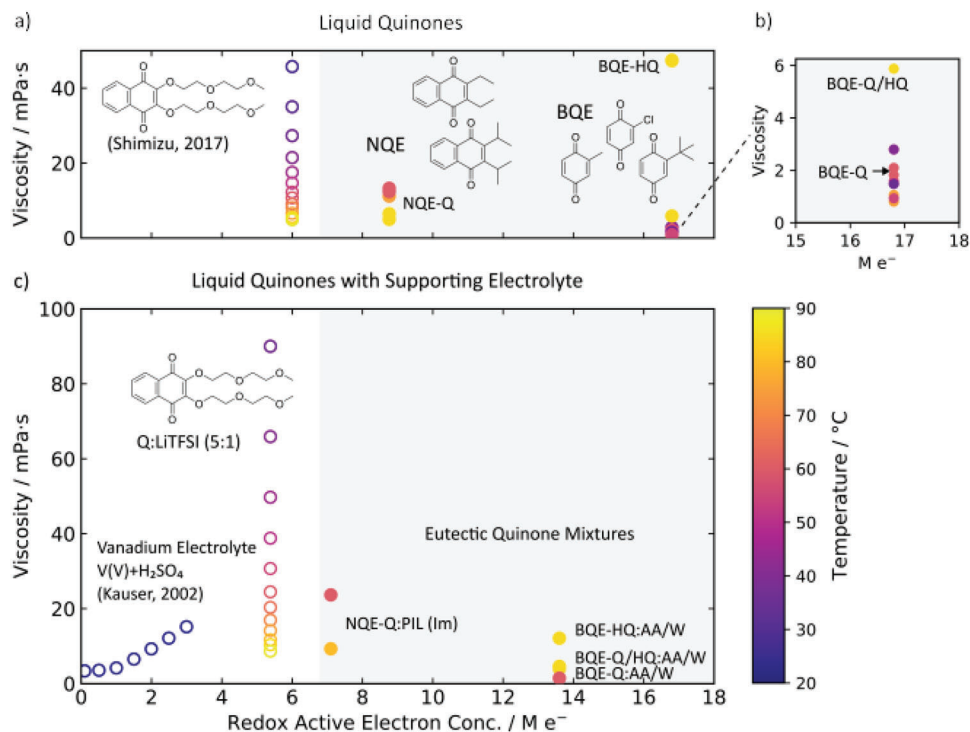


Figure 24. The viscosity of liquid quinones is plotted against the redox-active electron concentration for various quinone-based electrolytes. The data includes eutectic quinone electrolytes done by Emily Penn et al.'s work (represented by filled circles) and data from other literature for comparison with solvent-led and molecular engineering approaches (represented by open circles). a) The graph shows different liquid quinones, including the naphthoquinone eutectic (NQE) system, benzoquinone eutectic (BQE), and a glycolated naphthoquinone liquid obtained through molecular engineering. The quinone and hydroquinone forms of the mixture are indicated by -Q and -HQ, respectively, while -Q/HQ represents a 1:1 mixture of the quinone and hydroquinone forms. The inset (b) highlights the low viscosity of single-component benzoquinones and the BQE mixture in the BQE-Q and BQE-Q/HQ compositions. c) The graph compares liquid quinones with supporting electrolyte. For the eutectic quinone mixtures, NQE-Q: PIL represents the oxidized form of the NQE mixed with an imidazole-imidazolium TFSI NSPIL in a 5:1 ratio. BQE-Q: AA/W indicates a mixture of the BQE with acetic acid and water in a 10:5:1 molar ratio. The graph also includes a comparison with a molecular engineering approach using a glycolated liquid naphthoquinone with LiTFSI in a 5:1 molar ratio, as well as a solvent-led approach using a vanadium electrolyte $V_2(SO_4)_5$ with a 5 M total sulfates concentration. Reproduced with permission.^[124] Copyright 2023, American Chemical Society.

quinone–hydroquinone redox pairs, they provide a viable option for enhancing conductivity in quinone systems using alkali metal salts and the TFSI anion (Figure 25).^[122]

The left figure illustrates the ionic conductivity of liquid naphthoquinones in the presence of different supporting electrolytes. The compositions of the mixtures are indicated as molar ratios. Specifically, the first composition, NQ:HCl 5.125:1, consists of 2,3-diethyl-1,4-naphthoquinone (DENQ), 2,3-diisopropyl-1,4-naphthoquinone (DIPNQ), and hydroquinone analogues of DENQ (DENQH) in a ratio of 5:5:0.25, with hydrochloric acid (HCl) as the supporting electrolyte. The second composition, NQ:ImImTFSI 5:1, comprises DENQ and DIPNQ in a 1:1 ratio, representing the NQE composition, with imidazole-imidazolium bis(trifluoromethanesulfonyl)imide (ImImTFSI) as the supporting electrolyte. The third composition, NQ:PyrPyrTFSI 5:1, combines DENQ with pyrrolidinium bis(trifluoromethanesulfonyl)imide (PyrPyrTFSI) in a 5:1 ratio. Lastly, the fourth composition, NQ:PyrPyrTFSI 5.1:1, consists of DENQ and DENQH in a ratio of 10:1, with PyrPyrTFSI as the supporting electrolyte.

The right figure demonstrates the ionic conductivity of 1 M salts in an equimolar mixture of Q2-Q3-Q5 (2-methyl-

1,4-benzoquinone, 2,6-dimethylbenzoquinone, and 2-*tert*-butyl-1,4-benzoquinone). The tested salts include potassium bis(trifluoromethanesulfonyl)imide (KTFSI), sodium bis(trifluoromethanesulfonyl)imide (NaTFSI), and lithium bis(trifluoromethanesulfonyl)imide (LiTFSI). Although other salts such as potassium chloride, potassium acetate, hydroquinone sulfonic acid potassium salt, 1,2-naphthoquinone-4-sulfonic acid sodium salt, and anthraquinone-2,7-disulfonic acid disodium salt were also tested, their measured ionic conductivity was negligible or below the instrument noise level.

Enhancing ionic conductivity relies on several crucial factors that need to be considered:

Electrolyte Optimization: Choose appropriate supporting electrolytes and explore alternative salt combinations and ionic liquids to enhance conductivity. Understanding the mechanisms of ion transport within the electrolyte and across the membranes is crucial. Different transport mechanisms, such as diffusion, migration, and convection, can influence ionic conductivity. Optimizing the design and materials based on these mechanisms can lead to improved conductivity.

Solvent Selection: Select solvents with good solubility for quinone compounds and the supporting electrolyte. Consider

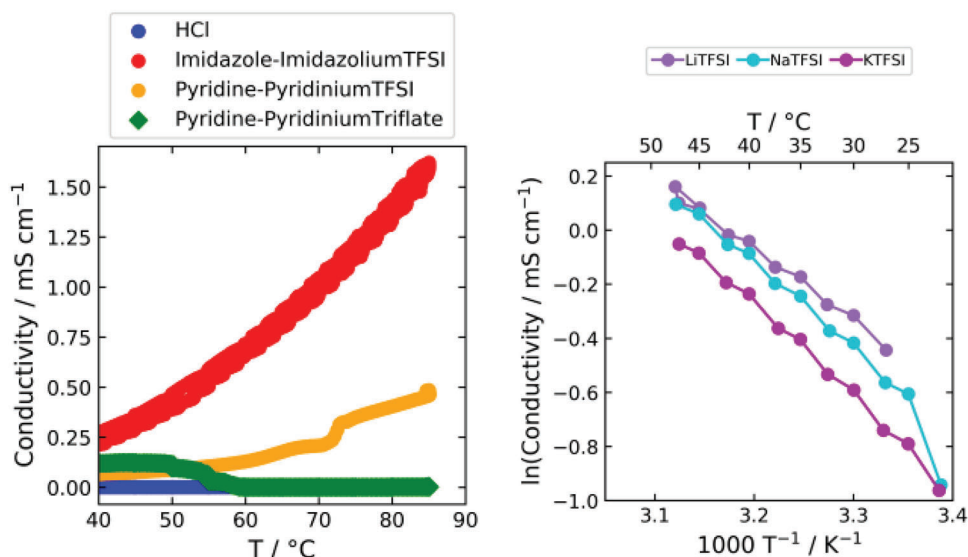


Figure 25. The left figure depicts the ionic conductivity of liquid naphthoquinones with various supporting electrolytes. The right figure demonstrates the ionic conductivity of 1 M salts (KTFSI, NaTFSI, LiTFSI) dissolved in an equimolar mixture of Q2-Q3-Q5. Reproduced with permission.^[124] Copyright 2023, American Chemical Society.

using mixed solvents or co-solvents to promote better ion transport. Maintaining the appropriate pH and employing pH buffering systems can optimize ionic conductivity. The pH can influence the dissociation of ions and the overall electrochemical reactions. Buffering systems can help maintain the desired pH range during battery operation.

Quinone Structure Modification: Modify the molecular structure of quinone compounds to enhance solubility and ion mobility. Introduce functional groups or substituents that increase solubility while considering the impact on redox potential and stability.

Electrode Design: Optimize electrode materials, such as carbon-based materials or conductive polymers, to enhance ion transport and facilitate faster charge/discharge processes. Maximize ion accessibility through electrode architecture design.

Membrane Selection: Choose ion-selective membranes with low resistance and good selectivity to maintain high ionic conductivity and prevent cross-contamination.

Temperature Control: Control the operating temperature within an optimal range to enhance ion mobility and reduce resistance. Ensure compatibility of electrolyte, membrane, and components with the desired temperature.

7. The Collection of Quinones in a Combinatorial Library

In order to investigate the electrochemical properties of potential quinones, we have shown a virtual library of molecules by modifying the central structures of quinones and introducing diverse chemical substituents onto their cores reported by Süleyman Er et al. The library encompasses various classes of quinones based on the number of rings present, namely, one-, two-, and three-ring isomers. These isomers are categorized according to the placement of ketone groups on the quinone frameworks. In addition, screening library includes multiple-ring quinone isomers

where the two cyclic ketone groups are located on different rings. Consequently, the combinatorial library of pure quinones comprises two, six, and nine distinct classes for BQs, NQs, and AQs, respectively (Figure 26)

Here, they have shown a range of R-groups as substituents, including $-\text{N}(\text{CH}_3)_2$, $-\text{NH}_2$, $-\text{OCH}_3$, $-\text{OH}$, $-\text{SH}$, $-\text{CH}_3$, $-\text{SiH}_3$, $-\text{F}$, $-\text{Cl}$, $-\text{C}_2\text{H}_5$, $-\text{CHO}$, $-\text{COOCH}_3$, $-\text{CF}_3$, $-\text{CN}$, $-\text{COOH}$, $-\text{PO}_3\text{H}_2$, $-\text{SO}_3\text{H}$, and $-\text{NO}_2$. The position of these substituents is known to have a significant impact on the electrochemical properties of quinones, as demonstrated in previous studies.^[87,32,142–144] The combinatorial quinone library consists of a total of 1710 molecular couples, encompassing both quinones (Q) and hydroquinone (QH₂).

The creation of a combinatorial library of quinones, as described in the research by Süleyman Er et al., provides a valuable resource for the development of future quinones for aqueous redox flow batteries. By modifying the central structures of quinones and introducing diverse chemical substituents onto their cores, this virtual library offers a wide range of potential quinone molecules with varying properties and characteristics. The availability of such a diverse quinone library allows for systematic screening and evaluation of the electrochemical properties of different quinone molecules. Researchers can assess factors such as redox potential, solubility, stability, and kinetics of these molecules in aqueous electrolytes. Through this screening process, promising quinones with desirable properties for redox flow battery applications can be identified.

The combinatorial library serves as a valuable tool for understanding the structure–property relationships of quinones and guiding the design and synthesis of future quinones tailored specifically for aqueous redox flow batteries.^[33,145–147] It facilitates the exploration of novel quinone structures, substitution patterns, and functional groups that may lead to improved performance, enhanced stability, and increased energy efficiency in redox flow battery systems.

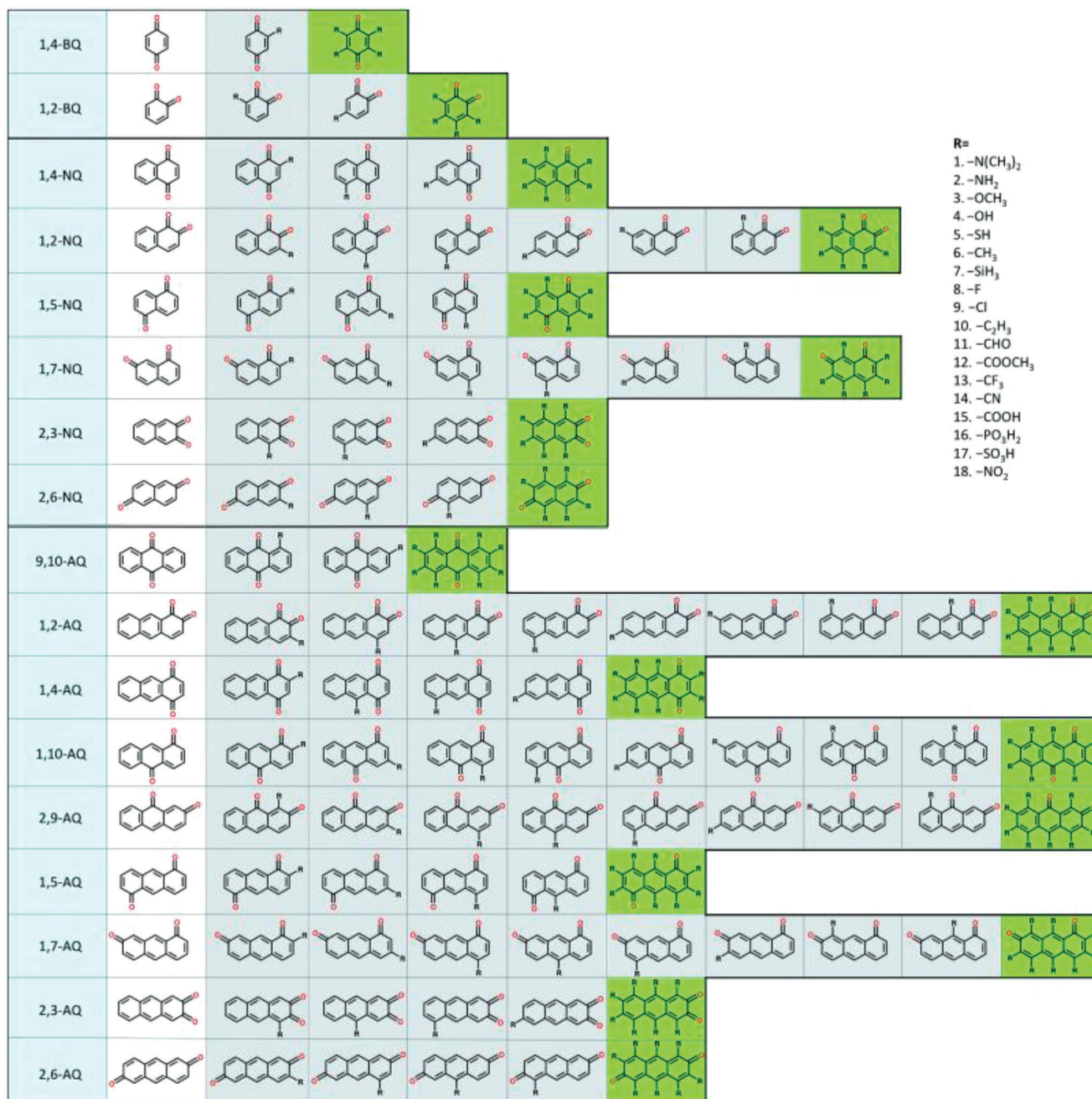


Figure 26. The molecular screening library is depicted in a schematic representation. On the left side, the original benzoquinone (BQ), naphthoquinone (NQ), and anthraquinone (AQ) isomers are illustrated in white. To expand the library, these quinone isomers are modified with 18 distinct R-groups individually (gray) and completely (green), resulting in a total of 1710 unique quinone molecules. Reproduced with permission.^[43] Copyright 2015, The Royal Society of Chemistry.

During the period from 2020 to 2022, remarkable strides have been made in the exploration and application of star quinone-based molecules for AORFBs (Figure 27). Researchers have successfully capitalized on the versatile nature of quinone structures by introducing diverse modifications, thereby fine-tuning their redox potentials to cater to specific requirements in varying electrochemical environments. This exceptional structural diversity enables the optimization of performance and compat-

ibility with selected reference electrode systems. Through the strategic utilization of the structural diversity and designability of quinone-based molecules, coupled with computational tools and informed choices of electrolytes, significant advancements have been achieved in the advancement of AORFBs. These endeavors have led to the identification and utilization of star quinone-based molecules that exhibit tailored redox potentials for targeted electrochemical environments. These breakthroughs have been

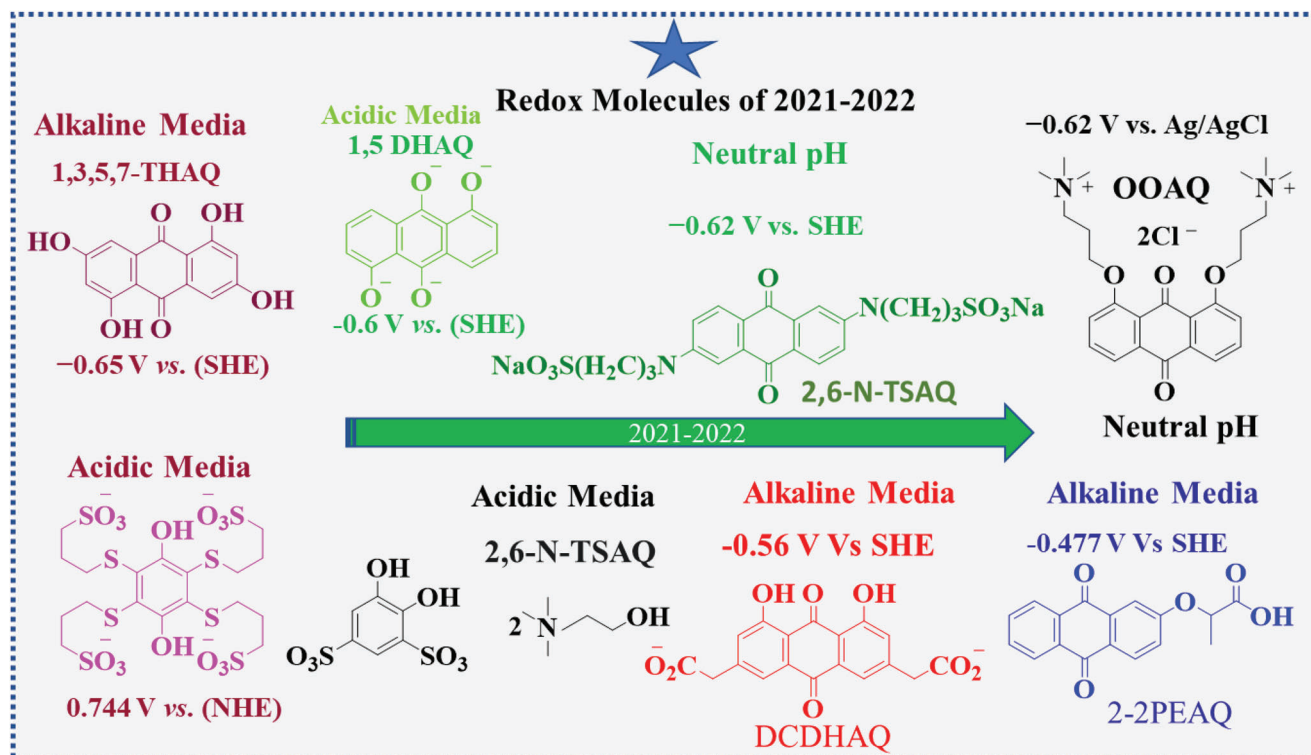


Figure 27. Aqueous organic redox flow batteries (AORFBs) use various quinone-based organic redox species as electroactive materials. These species exhibit different redox potentials relative to the standard hydrogen electrode (SHE), normal hydrogen electrode (NHE), and Ag/AgCl in acidic, neutral, and alkaline environments, respectively.^[86,94,148–151]

instrumental in advancing aqueous redox flow battery technology, ushering in new possibilities for efficient and sustainable energy storage solutions.

The relationship between quinone structures and their properties in the context of RFB applications is a topic of active research. Recent publications have provided valuable insights into the impact of structural modifications on redox potential, solubility, stability, and kinetics of quinones. These findings contribute to the rational design and optimization of quinone-based molecules for enhanced performance in RFBs. By tailoring the structure–property relationships, researchers strive to develop quinones with improved energy storage capacity, solubility, stability, and power density, paving the way for the advancement of efficient and sustainable redox flow battery technologies.

8. Summary and Future Directions

The development of commercially viable quinone-based RFBs still faces significant challenges. Compared to vanadium systems, the lifetime of various organic systems falls short of the required criteria for advanced quinone-based RFBs. These criteria include a cell voltage of over ≈ 1.0 V, aqueous solubility of around 1 M (equivalent to 27 Ah L⁻¹ of electrons), favorable redox kinetics (kinetic ASR \ll membrane ASR), and chemical stability with a fade rate of $< \approx 10\%$ year⁻¹.

Efforts have been made to enhance the stability of benzoquinones, but more research is needed to optimize and stabilize them for practical application in RFBs. Substituting benzo-

quinones with appropriate substituents may increase their redox potential and solubility while preventing degradation. Naphthoquinones are also in the early stages of research for their potential application in RFBs. Anthraquinone-based flow batteries coupled with ferri/ferrocyanide systems show promise in terms of stability. However, the economic prospects need to be carefully considered, as the cost of starting materials, reagents, and synthetic routes can sometimes be expensive and hinder the goal of achieving low-cost RFBs. For instance, a report by Gregory et al. mentioned a sales price of approximately 50 USD/kWh for an AQDS anolyte combined with sodium ferrocyanide catholyte, which is double the target set by the U.S. Department of Energy. To improve the economics of quinone-based RFBs, several criteria should be followed. The battery should operate at a voltage higher than 1.5 V, the organic redox active species should have a low mass per equivalent (less than 100 g equivalent⁻¹), and cost-effective sourcing of raw materials and development of less expensive synthetic routes should be pursued.^[152] Moreover, the engineering aspects such as test of kW-level stacks, their capacity decay rate study, efficiency test, flow rate optimization should also be focus on. Despite the significant progress in the development of quinones-based redox flow batteries (QORFBs), there are still several challenges that need to be addressed to improve their performance, including capacity, stability, Supporting electrolyte, cell voltage, and efficiencies.

The development of commercially viable quinone-based RFBs faces challenges related to stability, cell voltage, capacity, and cost-effectiveness. One major challenge is the limited stability

of quinones in high-potential electrolytes, resulting in low overall cell voltages. Efforts are being made to enhance stability by substituting benzoquinones with appropriate functional groups and exploring naphthoquinones for their potential application in RFBs. Molecular engineering strategies are being employed to improve stability by incorporating π -conjugated extensions, designing systems with stable radicals or nonradicals, utilizing hydrogen bond effects, mitigating crossover of redox species, and implementing the O₂-balance strategy. These approaches aim to reduce degradation mechanisms and prolong cycle life. To achieve high-voltage QORFBs, stable redox species with a large potential gap are required. However, challenges associated with water splitting reactions at high voltages need to be addressed for stability. Enhancing the solubility of organic redox-active materials is essential for achieving high-capacity QORFBs. Strategies include incorporating hydrophilic functional groups, breaking the symmetry of molecular structures, replacing counter ions, and smart choice of supporting electrolytes. The economic prospects of QORFBs need to be considered, and cost-effective sourcing of raw materials, less expensive synthetic routes, and low mass per equivalent redox-active species are important for improving their economics. Engineering aspects such as testing kW-level stacks, studying capacity decay rate, optimizing flow rate, and assessing efficiency also play a crucial role.

While advancements have been made in the cycling stability of QORFBs, the energy density of these systems needs improvement to compete with traditional inorganic RFBs. The sensitivity of organic radicals to oxygen limits their operation under ambient air conditions. Developing organic redox molecules with high water solubility, high stability, low cost, and air stability across all redox states is essential. advanced characterization methods and computational techniques can provide insights into redox reaction mechanisms and capacity fade mechanisms in QORFBs. High-throughput computational techniques like DFT calculations can aid in the selection and design of ideal organic redox species. The utilization of pH-neutral or weak alkaline electrolytes shows promise for QORFBs as it mitigates corrosion, undesired side reactions, and improves the solubility of quinones. by optimizing the properties and design of quinones-based redox-active materials, researchers can work toward safe, clean, and sustainable grid energy storage solutions.

In conclusion, the molecular engineering of quinones-based redox-active materials holds significant potential for addressing the challenges of capacity, stability, cell voltage, and efficiencies in QORFBs. By optimizing the electrochemical window, supporting electrolytes, ionic liquid properties and design of quinones, researchers can strive toward safe, clean, and sustainable grid energy storage solutions. The information provided by this review articles can be utilized to establish correlations between material properties and structure. These correlations can serve as a basis for exploring potential new materials for Aqueous RFBs, thereby advancing the field and addressing the current challenges.

Acknowledgements

This research was supported by the Nanoscale science Ph.D Program, Department of Chemistry at the University of North Carolina at Charlotte. All authors contributed equally in this paper.

Conflict of Interest

The authors declare no conflict of interest.

Keywords

chemical stability, electrolytes, quinones, redox potential, solubility limit

Received: April 4, 2023
Revised: June 14, 2023
Published online: July 17, 2023

- [1] A. Castillo, D. F. Gayme, *Energy Convers. Manage.* **2014**, *87*, 885.
- [2] A. R. Dehghani-Sanij, E. Tharumalingam, M. B. Dusseault, R. Fraser, *Renewable Sustainable Energy Rev.* **2019**, *104*, 192.
- [3] H. Mostafa, A. M. Ahmed, M. Shaban, A. A. Abdel-Khaliek, F. Hasan, F. Mohammed Alzahrani, M. Rabia, *Photonics* **2022**, *9*, 968.
- [4] F. Hasan, J. Kim, H. Song, S. H. Lee, J. H. Sung, J. Kim, H. D. Yoo, *J. Electrochem. Sci. Technol.* **2020**, *11*, 352.
- [5] O. Ellabban, H. Abu-Rub, F. Blaabjerg, *Renewable Sustainable Energy Rev.* **2014**, *39*, 748.
- [6] T. T. D. Tran, A. D. Smith, *Renewable Sustainable Energy Rev.* **2017**, *80*, 1372.
- [7] I. Dincer, C. Acar, *Int. J. Energy Res.* **2015**, *39*, 585.
- [8] A. A. A. Abdelazeez, A. B. G. Trabelsi, F. H. Alkallas, M. Rabia, *Sol. Energy* **2022**, *248*, 251.
- [9] F. Hasan, A. A. A. Abdelazeez, M. Rabia, H. D. Yoo, *Energy Technol.* **2023**, *11*, 2300153.
- [10] J. H. Sung, T. W. Kim, H.-K. Kang, S. Y. Choi, F. Hasan, S. K. Mohanty, J. Kim, M. K. Srinivasa, H.-C. Shin, H. D. Yoo, *Korean J. Chem. Eng.* **2021**, *38*, 1059.
- [11] Y. Tian, G. Zeng, A. Rutt, T. Shi, H. Kim, J. Wang, J. Koettgen, Y. Sun, B. Ouyang, T. Chen, Z. Lun, Z. Rong, K. Persson, G. Ceder, *Chem. Rev.* **2020**, *121*, 1623.
- [12] M. A. Pellow, H. Ambrose, D. Mulvaney, R. Betita, S. Shaw, *Sustainable Mater. Technol.* **2020**, *23*, e00120.
- [13] K. Y. Kwon, T. H. Jo, J. S. Kim, F. Hasan, H. D. Yoo, *ACS Appl. Mater. Interfaces* **2020**, *12*, 42612.
- [14] B. Dunn, H. Kamath, J.-M. Tarascon, *Science* **2011**, *334*, 928.
- [15] T. Faunce, J. Prest, D. Su, S. Hearne, F. Iacopi, *MRS Energy Sustainability* **2018**, *5*, E11.
- [16] J. Winsberg, T. Hagemann, T. Janoschka, M. D. Hager, U. S. Schubert, *Angew. Chem., Int. Ed.* **2017**, *56*, 686.
- [17] B. Li, J. Liu, *Natl. Sci. Rev.* **2017**, *4*, 91.
- [18] L. Zhang, R. Feng, W. Wang, G. Yu, *Nat. Rev. Chem.* **2022**, *6*, 524.
- [19] Y. Ding, C. Zhang, L. Zhang, Y. Zhou, G. Yu, *Chem* **2019**, *5*, 1964.
- [20] W. Wang, W. Xu, L. Cosimbescu, D. Choi, L. Li, Z. Yang, *Chem. Commun.* **2012**, *48*, 6669.
- [21] N. A. Turner, M. B. Freeman, H. D. Pratt, A. E. Crockett, D. S. Jones, M. R. Anstey, T. M. Anderson, C. M. Bejger, *Chem. Commun.* **2020**, *56*, 2739.
- [22] H. Chen, G. Cong, Y.-C. Lu, *J. Energy Chem.* **2018**, *27*, 1304.
- [23] M. V. Holland-Cunz, F. Cording, J. Friedl, U. Stimming, *Front. Energy* **2018**, *12*, 198.
- [24] Y. Ding, C. Zhang, L. Zhang, Y. Zhou, G. Yu, *Chem. Soc. Rev.* **2018**, *47*, 69.
- [25] J. A. Kowalski, L. Su, J. D. Milshtein, F. R. Brushett, *Curr. Opin. Chem. Eng.* **2016**, *13*, 45.
- [26] L. Briot, M. Petit, Q. Cacciuto, M.-C. Pera, *J. Power Sources* **2022**, *536*, 231427.

- [27] P. Leung, T. Martin, Q. Xu, C. Flox, M. R. Mohamad, J. Palma, A. Rodchanarowan, X. Zhu, W. W. Xing, A. A. Shah, *Appl. Energy* **2021**, 282, 116058.
- [28] V. Singh, S. Kim, J. Kang, H. R. Byon, *Nano Res.* **2019**, 12, 1988.
- [29] A. M. Kosswattaarachchi, T. R. Cook, *Electrochim. Acta* **2018**, 261, 296.
- [30] F. Zhang, M. Cazot, G. Maranzana, J. Dillet, S. Didierjean, *J. Energy Storage* **2022**, 55, 105704.
- [31] S. Lee, J. Hong, K. Kang, *Adv. Energy Mater.* **2020**, 10, 2001445.
- [32] Y. Jing, R. G. Gordon, M. J. Aziz, *Flow Batteries: From Fundamentals to Applications*, Vol. 3, Wiley Online Library, Germany **2023**, pp. 895–922.
- [33] A. Khetan, *Batteries* **2023**, 9, 24.
- [34] D. Chao, W. Zhou, F. Xie, C. Ye, H. Li, M. Jaroniec, S.-Z. Qiao, *Sci. Adv.* **2020**, 6, eaba4098.
- [35] C. Zhang, L. Zhang, Yu Ding, S. Peng, X. Guo, Yu Zhao, G. He, G. Yu, *Energy Storage Mater.* **2018**, 15, 324.
- [36] S. S. SV, J. N. Law, C. E. Tripp, *Nat. Mach. Intell.* **2022**, 4, 720.
- [37] D. G. Kwabi, Y. Ji, M. J. Aziz, *Chem. Rev.* **2020**, 120, 6467.
- [38] X. Wei, W. Pan, W. Duan, A. Hollas, Z. Yang, B. Li, Z. Nie, J. Liu, D. Reed, W. Wang, V. Sprenkle, *ACS Energy Lett.* **2017**, 2, 2187.
- [39] M. Park, J. Ryu, W. Wang, J. Cho, *Nat. Rev. Mater.* **2016**, 2, 1.
- [40] G. Yang, Y. Zhu, Z. Hao, Y. Lu, Q. Zhao, K. Zhang, J. Chen, *Adv. Mater.* **2023**, 35, 2301898.
- [41] D. R. Weinberg, C. J. Gagliardi, J. F. Hull, C. F. Murphy, C. A. Kent, B. C. Westlake, A. Paul, D. H. Ess, D. G. McCafferty, T. J. Meyer, *Chem. Rev.* **2012**, 112, 4016.
- [42] K. Wedege, E. Dražević, D. Konya, A. Bientien, *Sci. Rep.* **2016**, 6, 39101.
- [43] S. Er, C. Suh, M. P. Marshak, A. Aspuru-Guzik, *Chem. Sci.* **2015**, 6, 885.
- [44] M. Pan, M. Shao, Z. Jin, *SmartMat* **2023**, e1198.
- [45] J. Kim, Y. Kim, J. Yoo, G. Kwon, Y. Ko, K. Kang, *Nat. Rev. Mater.* **2023**, 8, 54.
- [46] X. Fang, L. Zeng, Z. Li, L. A. Robertson, I. A. Shkrob, Lu Zhang, X. Wei, *Next Energy* **2023**, 1, 100008.
- [47] C. G. Cannon, P. A. A. Klusener, N. P. Brandon, A. Kucernak, *ChemSusChem* **2023**, 16, 202300303.
- [48] G. Mandouma, J. Collins, D. Williams, *Acc. Chem. Res.* **2023**, 56, 1263.
- [49] R. Rubio-Presa, L. Lubián, M. Borlaf, E. Ventosa, R. Sanz, *ACS Mater. Lett.* **2023**, 5, 798.
- [50] W. Hu, Y. Peng, Y. Wei, Y. Yang, *J. Phys. Chem. C* **2023**, 127, 4465.
- [51] K. Liu, Z. Wei, C. Zhang, Y. Shang, R. Teodorescu, Q.-L. Han, *IEEE/CAA J. Autom. Sin.* **2022**, 9, 1139.
- [52] X. Yang, S. Garcia, T. Janoschka, D. Kónya, M. Hager, U. Schubert, *Molecules* **2021**, 26, 3823.
- [53] A. Hashemi, R. Khakpour, A. Mahdian, M. Busch, P. Peljo, K. Laasonen, *chemRxiv*, **2023**.
- [54] S. Ghule, S. R. Dash, S. Bagchi, K. Joshi, K. Vanka, *ACS Omega* **2022**, 7, 11742.
- [55] R. P. Fornari, P. de Silva, *Molecules* **2021**, 26, 3978.
- [56] J. M. Cameron, C. Holc, A. J. Kibler, C. L. Peake, D. A. Walsh, G. N. Newton, L. R. Johnson, *Chem. Soc. Rev.* **2021**, 50, 5863.
- [57] O. Nolte, I. A. Volodin, C. Stolze, M. D. Hager, U. S. Schubert, *Mater. Horiz.* **2021**, 8, 1866.
- [58] H. Peng, Q. Yu, S. Wang, J. Kim, A. E. Rowan, A. K. Nanjundan, Y. Yamauchi, J. Yu, *Adv. Sci.* **2019**, 6, 1900431.
- [59] C. Han, H. Li, R. Shi, T. Zhang, J. Tong, J. Li, B. Li, *J. Mater. Chem. A* **2019**, 7, 23378.
- [60] Y. Lu, Q. Zhang, L. Li, Z. Niu, J. Chen, *Chem* **2018**, 4, 2786.
- [61] P. Deng, C. Zhou, Y. Wei, X. Yue, J. Li, L. Yao, J. Ding, Q. He, *J. Electroanal. Chem.* **2022**, 918, 116506.
- [62] A. Murali, A. Nirmalchandar, S. Krishnamoorthy, L. Hooper-Burkhardt, B. Yang, G. Soloveichik, G. K. S. Prakash, S. R. Narayanan, *J. Electrochem. Soc.* **2018**, 165, A1193.
- [63] J.-M. Fontmorin, S. Guiheneuf, T. Godet-Bar, D. Floner, F. Geneste, *Curr. Opin. Colloid Interface Sci.* **2022**, 101624.
- [64] B. Yang, L. Hooper-Burkhardt, F. Wang, G. K. S. Prakash, S. R. Narayanan, *J. Electrochem. Soc.* **2014**, 161, A1371.
- [65] L. Hooper-Burkhardt, S. Krishnamoorthy, B. Yang, A. Murali, A. Nirmalchandar, G. K. S. Prakash, S. R. Narayanan, *J. Electrochem. Soc.* **2017**, 164, A600.
- [66] W. Schlemmer, P. Nothdurft, A. Petzold, G. Riess, P. Frühwirth, M. Schmallegger, G. Gescheidt-Demner, R. Fischer, S. A. Freunberger, W. Kern, S. Spirk, *Angew. Chem., Int. Ed.* **2020**, 59, 22943.
- [67] Q. Liu, X. Li, C. Yan, A. Tang, *J. Power Sources* **2020**, 460, 228124.
- [68] S. Schindler, T. Bechtold, *J. Electroanal. Chem.* **2019**, 836, 94.
- [69] V. Mahanta, K. Ramanujam, *J. Electrochem. Soc.* **2022**, 169, 030525.
- [70] W. Wu, J. Luo, F. Wang, B. Yuan, T. L. Liu, *ACS Energy Lett.* **2021**, 6, 2891.
- [71] V. Mahanta, R. Gupta, K. Ramanujam, *ACS Appl. Energy Mater.* **2022**, 5, 15166.
- [72] E. Drazevic, C. Szabo, D. Konya, T. Lund, K. Wedege, A. Bientien, *ACS Appl. Energy Mater.* **2019**, 2, 4745.
- [73] D. Xu, C. Zhang, Y. Zhen, Y. Li, *ACS Appl. Energy Mater.* **2021**, 4, 8045.
- [74] X. Li, P. Gao, Y.-Y. Lai, J. D. Bazak, A. Hollas, H.-Y. Lin, V. Murugesan, S. Zhang, C.-F. Cheng, W.-Y. Tung, Y.-T. Lai, R. Feng, J. Wang, C.-L. Wang, W. Wang, Y. Zhu, *Nat. Energy* **2021**, 6, 873.
- [75] Z. Zhao, C. Zhang, X. Li, *J. Energy Chem.* **2022**, 67, 621.
- [76] M. Park, E. S. Beh, E. M. Fell, Y. Jing, E. F. Kerr, D. Porcellinis, M.-A. Goulet, J. Ryu, A. A. Wong, R. G. Gordon, J. Cho, M. J. Aziz, *Adv. Energy Mater.* **2019**, 9, 1900694.
- [77] J. Sivanadanam, R. Murugan, H. Khan, I. S. Aidhen, K. Ramanujam, *J. Electrochem. Soc.* **2022**, 169, 020533.
- [78] B. Hu, C. Debruler, Z. Rhodes, T. L. Liu, *J. Am. Chem. Soc.* **2017**, 139, 1207.
- [79] T. Janoschka, N. Martin, M. D. Hager, U. S. Schubert, *Angew. Chem., Int. Ed.* **2016**, 55, 14427.
- [80] S. Jin, Y. Jing, D. G. Kwabi, Y. Ji, L. Tong, D. De Porcellinis, M.-A. Goulet, D. A. Pollack, R. G. Gordon, M. J. Aziz, *ACS Energy Lett.* **2019**, 4, 1342.
- [81] M. Chou, *Prog. Polym. Sci.* **2003**, 28, 1223.
- [82] P. Hu, H. Lan, X. Wang, Y. Yang, X. Liu, H. Wang, L. Guo, *Energy Storage Mater.* **2019**, 19, 62.
- [83] L. Tong, M.-A. Goulet, D. P. Tabor, E. F. Kerr, D. De Porcellinis, E. M. Fell, A. Aspuru-Guzik, R. G. Gordon, M. J. Aziz, *ACS Energy Lett.* **2019**, 4, 1880.
- [84] D. Pinheiro, M. Pineiro, J. S. S. De Melo, *Commun. Chem.* **2021**, 4, 89.
- [85] J. Carretero-González, E. Castillo-Martínez, M. Armand, *Energy Environ. Sci.* **2016**, 9, 3521.
- [86] Y. Zhu, Y. Li, Y. Qian, L. Zhang, J. Ye, X. Zhang, Y. Zhao, *J. Power Sources* **2021**, 501, 229984.
- [87] Y. Jing, E. M. Fell, M. Wu, S. Jin, Y. Ji, D. A. Pollack, Z. Tang, D. Ding, M. Bahari, M.-A. Goulet, T. Tsukamoto, R. G. Gordon, M. J. Aziz, *ACS Energy Lett.* **2022**, 7, 226.
- [88] J. Mao, W. Ruan, Q. Chen, *J. Electrochem. Soc.* **2020**, 167, 070522.
- [89] J. Cao, M. Tao, H. Chen, J. Xu, Z. Chen, *J. Power Sources* **2018**, 386, 40.
- [90] L. Xia, W. Huo, H. Gao, H. Zhang, F. Chu, H. Liu, Z. Tan, *J. Power Sources* **2021**, 498, 229896.
- [91] C. Wang, B. Yu, Y. Liu, H. Wang, Z. Zhang, C. Xie, X. Li, H. Zhang, Z. Jin, *Energy Storage Mater.* **2021**, 36, 417.
- [92] S. Guiheneuf, T. Godet-Bar, J.-M. Fontmorin, C. Jourdin, D. Floner, F. Geneste, *J. Power Sources* **2022**, 539, 231600.

- [93] Y. Jing, E. M. Fell, M. Wu, S. Jin, Y. Ji, D. A. Pollack, Z. Tang, D. Ding, M. Bahari, M.-A. Goulet, T. Tsukamoto, R. G. Gordon, M. J. Aziz, *ACS Energy Lett.* **2021**, *7*, 226.
- [94] M. Wu, M. Bahari, E. M. Fell, R. G. Gordon, M. J. Aziz, *J. Mater. Chem. A* **2021**, *9*, 26709.
- [95] M. Wu, Y. Jing, A. A. Wong, E. M. Fell, S. Jin, Z. Tang, R. G. Gordon, M. J. Aziz, *Chem* **2020**, *6*, 1432.
- [96] W. Lee, A. Permatasari, Y. Kwon, *J. Mater. Chem. C* **2020**, *8*, 5727.
- [97] Y. Jing, E. W. Zhao, M.-A. Goulet, M. Bahari, E. M. Fell, S. Jin, A. Davoodi, E. Jónsson, M. Wu, C. P. Grey, R. G. Gordon, M. J. Aziz, *Nat. Chem.* **2022**, *14*, 1103.
- [98] Y. Ji, M.-A. Goulet, D. A. Pollack, D. G. Kwabi, S. Jin, D. Porcellinis, E. F. Kerr, R. G. Gordon, M. J. Aziz, *Adv. Energy Mater.* **2019**, *9*, 1900039.
- [99] D. G. Kwabi, K. Lin, Y. Ji, E. F. Kerr, M.-A. Goulet, D. De Porcellinis, D. P. Tabor, D. A. Pollack, A. Aspuru-Guzik, R. G. Gordon, M. J. Aziz, *Joule* **2018**, *2*, 1894.
- [100] S. Guiheneuf, A. Lê, T. Godet-Bar, L. Chancelier, J.-M. Fontmorin, D. Floner, F. Geneste, *ChemElectroChem* **2021**, *8*, 2526.
- [101] A. R. F. Lima, R. C. Pereira, J. Azevedo, A. Mendes, J. Sérgio Seixas De Melo, *J. Mol. Liq.* **2021**, *336*, 116364.
- [102] J. Chai, X. Wang, A. Lashgari, C. K. Williams, J. J. Jiang, *ChemSusChem* **2020**, *13*, 4069.
- [103] G. S. Nambafu, R. Siddharth, C. Zhang, T. Zhao, Q. Chen, K. Amine, M. Shao, *Nano Energy* **2021**, *89*, 106422.
- [104] E. S. Beh, D. De Porcellinis, R. L. Gracia, K. T. Xia, R. G. Gordon, M. J. Aziz, *ACS Energy Lett.* **2017**, *2*, 639.
- [105] Y. Ding, G. Yu, *Angew. Chem., Int. Ed.* **2017**, *56*, 8614.
- [106] T. Páez, A. Martínez-Cuevas, R. Marcilla, J. Palma, E. Ventosa, *J. Power Sources* **2021**, *512*, 230516.
- [107] Y. Yao, J. Lei, Y. Shi, F. Ai, Y.-C. Lu, *Nat. Energy* **2021**, *6*, 582.
- [108] R. Chen, *Chem. - Asian J.* **2023**, *18*, e202201024.
- [109] R. Chen, D. Bresser, M. Saraf, P. Gerlach, A. Balducci, S. Kunz, D. Schröder, S. Passerini, J. Chen, *ChemSusChem* **2020**, *13*, 2205.
- [110] M. Li, C. Wang, Z. Chen, K. Xu, J. Lu, *Chem. Rev.* **2020**, *120*, 6783.
- [111] Y. Yamada, J. Wang, S. Ko, E. Watanabe, A. Yamada, *Nat. Energy* **2019**, *4*, 269.
- [112] R. Chen, R. Hempelmann, *Electrochem. Commun.* **2016**, *70*, 56.
- [113] R. Ye, D. Henkensmeier, R. Chen, *Sustainable Energy Fuels* **2020**, *4*, 2998.
- [114] Z. Huang, C. W. M. Kay, B. Kuttich, D. Rauber, T. Kraus, H. Li, S. Kim, R. Chen, *Nano Energy* **2020**, *69*, 104464.
- [115] Z. Huang, R. Hempelmann, Y. Zhang, L. Tao, R. Chen, *Green Energy Environ.* **2022**, <https://doi.org/10.1016/j.ges.2022.09.005>.
- [116] Z. Huang, P. Zhang, X. Gao, D. Henkensmeier, S. Passerini, R. Chen, *ACS Appl. Energy Mater.* **2019**, *2*, 3773.
- [117] X. Wang, R. K. Gautam, J. J. Jiang, *Batteries Supercaps* **2022**, *5*, 202200298.
- [118] V. M. Ortiz-Martínez, L. Gómez-Coma, G. Pérez, A. Ortiz, I. Ortiz, *Sep. Purif. Technol.* **2020**, *252*, 117436.
- [119] A. Ejigu, P. A. Greatorex-Davies, D. A. Walsh, *Electrochem. Commun.* **2015**, *54*, 55.
- [120] M. Armand, F. Endres, D. R. Macfarlane, H. Ohno, B. Scrosati, *Nat. Mater.* **2009**, *8*, 621.
- [121] C. Xu, G. Yang, D. Wu, M. Yao, C. Xing, J. Zhang, H. Zhang, F. Li, Y. Feng, S. Qi, M. Zhuo, J. Ma, *Chem. - Asian J.* **2021**, *16*, 549.
- [122] L. Hu, L. i Gao, M. Di, X. Jiang, X. Wu, X. Yan, X. Li, G. He, *Energy Storage Mater.* **2021**, *34*, 648.
- [123] G. L. Soloveichik, *Chem. Rev.* **2015**, *115*, 11533.
- [124] E. Penn, A. Baclig, D. Ganapathi, W. C. Chueh, *Chem. Mater.* **2023**, *35*, <https://doi.org/10.1021/acs.chemmater.3c00156>.
- [125] C. Zhang, L. Zhang, G. Yu, *Acc. Chem. Res.* **2020**, *53*, 1648.
- [126] G. Cong, Y.-C. Lu, *Chem* **2018**, *4*, 2732.
- [127] A. C. Baclig, *Eutectic Liquids for High-Energy Density Flow Batteries*, Stanford University, California, USA **2019**.
- [128] V. P. Nemani, K. C. Smith, *J. Electrochem. Soc.* **2018**, *165*, A3144.
- [129] J. D. Milshtein, J. L. Barton, T. J. Carney, J. A. Kowalski, R. M. Darling, F. R. Brushett, *J. Electrochem. Soc.* **2017**, *164*, A2487.
- [130] J. D. Milshtein, R. M. Darling, J. Drake, M. L. Perry, F. R. Brushett, *J. Electrochem. Soc.* **2017**, *164*, A3883.
- [131] J. Zhang, R. E. Corman, J. K. Schuh, R. H. Ewoldt, I. A. Shkrob, L. u Zhang, *J. Phys. Chem. C* **2018**, *122*, 8159.
- [132] P. Galek, A. Slesinski, K. Fic, J. Menzel, *J. Mater. Chem. A* **2021**, *9*, 8644.
- [133] R. Chen, H. Zhang, F. Wu, *Prog. Chem.* **2011**, *23*, 366.
- [134] T. Liu, X. Wei, Z. Nie, V. Sprenkle, W. Wang, *Adv. Energy Mater.* **2016**, *6*, 1501449.
- [135] T. Janoschka, N. Martin, U. Martin, C. Friebe, S. Morgenstern, H. Hiller, M. D. Hager, U. S. Schubert, *Nature* **2015**, *527*, 78.
- [136] Q. Cheng, W. Fan, Y. He, P. Ma, S. Vanka, S. Fan, Z. Mi, D. Wang, *Adv. Mater.* **2017**, *29*, 1700312.
- [137] K. Lin, Q. Chen, M. R. Gerhardt, L. Tong, S. B. Kim, L. Eisenach, A. W. Valle, D. Hardee, R. G. Gordon, M. J. Aziz, M. P. Marshak, *Science* **2015**, *349*, 1529.
- [138] K. Wedege, J. Azevedo, A. Khataee, A. Bentien, A. Mendes, *Angew. Chem., Int. Ed.* **2016**, *55*, 7142.
- [139] M. Li, R. P. Hicks, Z. Chen, C. Luo, J. Guo, C. Wang, Y. Xu, *Chem. Rev.* **2023**, *123*, 1712.
- [140] H. Wang, R. Emanuelsson, C. Karlsson, P. Jannasch, M. Strømme, M. Sjödin, *ACS Appl. Mater. Interfaces* **2021**, *13*, 19099.
- [141] K. Qin, J. Huang, K. Holguin, C. Luo, *Energy Environ. Sci.* **2020**, *13*, 3950.
- [142] T. Y. George, E. F. Kerr, N. O. Haya, A. M. Alfaraidi, R. G. Gordon, M. J. Aziz, *J. Electrochem. Soc.* **2023**, *170*, 040509.
- [143] W. Ruan, J. Mao, Q. Chen, *Curr. Opin. Electrochem.* **2021**, *29*, 100748.
- [144] M. R. Gerhardt, et al., *Adv. Energy Mater.* **2017**, *7*, 1601488.
- [145] D. P. Tabor, L. M. Roch, S. K. Saikin, C. Kreisbeck, D. Sheberla, J. H. Montoya, S. Dwaraknath, M. Aykol, C. Ortiz, H. Tribukait, C. Amador-Bedolla, C. J. Brabec, B. Maruyama, K. A. Persson, A. Aspuru-Guzik, *Nat. Rev. Mater.* **2018**, *3*, 5.
- [146] Q. Zhang, A. Khetan, E. Sorkun, F. Niu, A. Loss, I. Pucher, S. Er, *Energy Storage Mater.* **2022**, *47*, 167.
- [147] E. Sorkun, Q. Zhang, A. Khetan, M. C. Sorkun, S. Er, *Scientific Data* **2022**, *9*, 718.
- [148] Z. Li, T. Jiang, M. Ali, C. Wu, W. Chen, *Energy Storage Mater.* **2022**, *50*, 105.
- [149] M. Pan, M. Shao, Z. Jin, *SmartMat* e1198.
- [150] K. Amini, E. F. Kerr, T. Y. George, A. M. Alfaraidi, Y. Jing, T. Tsukamoto, R. G. Gordon, M. J. Aziz, *Adv. Funct. Mater.* **2023**, *33*, 2211338.
- [151] M. Wu, et al., *Batteries Supercaps* **2022**, *5*, 202200009.
- [152] T. D. Gregory, M. L. Perry, P. Albertus, *J. Power Sources* **2021**, *499*, 229965.



Fuead Hasan is a graduate student currently pursuing Ph.D. in Nanoscale Science at the University of North Carolina at Charlotte, USA. His research primarily focuses on the field of energy storage systems, with a specific emphasis on exploring the potential of organic, Inorganic molecules, catholytes, anolytes for redox flow battery applications, high-capacity cathodes of lithium-ion batteries and metal-ion batteries. His expertise spans diverse areas, including materials synthesis and characterization, battery chemistry, and electrochemical analysis for research purposes. Hasan's unwavering enthusiasm lies in the development of cutting-edge and highly efficient energy storage technologies that can effectively tackle the pressing challenges faced by our modern world.